Eindhoven University of Technology

BACHELOR

Simulation of single fiber motion in complex fluids

Snepvangers, Anne-Wil G.M.M.

Award date:
2023

Link to publication

Disclaimer
This document contains a student thesis (bachelor's or master's), as authored by a student at Eindhoven University of Technology. Student theses are made available in the TU/e repository upon obtaining the required degree. The grade received is not published on the document as presented in the repository. The required complexity or quality of research of student theses may vary by program, and the required minimum study period may vary in duration.

General rights
Copyright and moral rights for the publications made accessible in the public portal are retained by the authors and/or other copyright owners and it is a condition of accessing publications that users recognise and abide by the legal requirements associated with these rights.

- Users may download and print one copy of any publication from the public portal for the purpose of private study or research.
- You may not further distribute the material or use it for any profit-making activity or commercial gain

Simulation of single fiber motion in complex fluids

Semester A - 2022-2023

Full Name	Student ID	Study
A.G.M.M. Snepvangers	1405020	Mechanical Engineering

Supervisor: Thijs Egelmeers & Nick Jaensson
Coordinator: Markus Hütter

Eindhoven, February 1, 2023

Contents

List of Symbols

Symbol	Quantity	Unit	
$\vec{q}$	Orientation vector	$[-]$	Dimensionless
ϕ	Relative angle of the projection of the orientation vector on the xy-plane from the y-axis	$[rad]$	Radians
θ	Relative angle from the z-axis	$[rad]$	Radians
ρ	Density	$[kg/m^3]$	Kilograms per cubic meter
v	Velocity	$[m/s]$	Meter per second
σ	Stress	$[kg/ms^2]$	Kilogram per meter second squared
b	Sum of the body forces	$[kgm/s^2]$	Kilogram meter per second squared
μ	Kinematic viscosity	$[kg/ms]$	Kilogram per meter second
η_s	Newtonian viscosity	$[kg/ms]$	Kilogram per meter second
p	Pressure	$[kg/ms^2]$	Kilogram per meter second squared
λ	Internal relaxation time	$[s]$	seconds
τ	Extra stress tensor	$[kg/ms^2]$	Kilogram per meter second squared
α	Non linear parameter	[-]	Dimensionless
η_p	Polymer viscosity	$[kg/ms]$	Kilogram per meter second
v^∞	Shear field	$[m^2/s]$	Meter squared per second
Δt	Time step	$[s]$	Seconds
t	Time	$[s]$	Seconds
$\dot{\gamma}$	Flow rate	$[m/s]$	Meter per second
r_e	Aspect ratio	[-]	Dimensionless
l	Length	$[m]$	Meter
d	Diameter	$[m]$	Meter
e	Absolute error	[-]	Dimensionless
ω_s	Angular velocity	$[rad/s]$	Radians per second

1 Introduction

Nowadays, many products are made using polymers. The reasons for this are, that polymers are lightweight, have low manufacturing cost, and are relatively easy to use during the manufacturing process. Polymers tend to have less strength compared to their steel counterparts [1]. During the shaping process of a product, adding hard fibers in the polymer melt can improve the total strength of the polymer product. These fibers have good properties in the axial direction, but not in the direction perpendicular to that axial direction [2]. Figure 1 shows the stress strain curve for two different samples. The red sample has fibers which are aligned with the load direction and the blue sample has fibers which are not aligned with the load direction. The stress strain behavior of these two sample is very different. This is caused by the orientation of these fibers.

The orientation of these fibers therefore greatly impacts the physical properties of the end product. During the processing of the polymer with the hard fibers, the local orientation of these fibers is determined by the fluid flow. For that reason, it is important to predict the fiber orientation kinetics during processing. When the orientation of the fibers is known, the mechanical properties can be predicted. A method to determine the orientation of the fibers in a product is by simulating what happens with fibers in certain fluid flows.

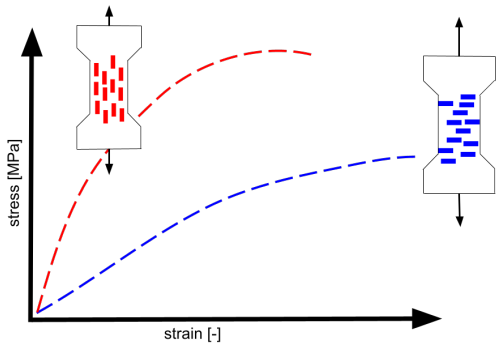

Figure 1: Stress strain curve for two different orientations of fibers

The aim of this work is to study the motion of a single fiber in complex (non-Newtonian) fluids utilizing Finite Element Method (FEM). The main focus is to find possible relations between the relevant polymer flow variables and how they affect the orientation of a single fiber. During the research, both extensional and shear flows are simulated around a hard fiber.

The report starts with a problem definition in Chapter 2. In Chapter 3 Jeffery orbits are introduced which analytically describe the motion of a single fiber in a Newtonian fluid. These equations will be used for the validation of the simulation software. In Chapter 4 the in-house FEM tool TFEM used to obtain the orientation of a single particle for a viscoelastic fluid will be explained. In Chapter 5 the results from the TFEM simulations will be validated with respect to the Jeffery orbits. In Chapter 6 the results of the simulations will be discussed.

2 Problem Definition

For most processing techniques of polymer melts are usually subjected to a combination of shear flows and extensional flows. An example of a shear flow for polymer melts is in 3D printing [3]. In 3D printing technology, parts are manufactured by the successively stacking of material layers. The material is deposited layer by layer, forming an end product. During film blowing of polymer, an extensional flow is exerted on the polymers [4]. During the film-blowing processes, pressurized gas is used to stretch the polymers. A typical product made by a film blowing process is garbage bags. To simplify these complex flows, in this report solely shear flow and uniaxial extensional flow are considered. Another simplification is that this report will look at the orientation kinetics of a single fiber rather than multiple fibers.

The orientation of a rod-like fiber in three dimensions can be described using an orientation vector

$$\vec{q} = q_x\vec{e_x} + q_y\vec{e_y} + q_z\vec{e_z}. \tag{1}$$

Where $\vec{e_x}$, $\vec{e_y}$, $\vec{e_z}$ are the unit vector in $x-$, $y-$ and $z-$direction respectfully, q_x, q_y and q_z are arbitrary scalars and $\vec{q}$ is the orientation vector, this vector has the property that the length is equal to 1.

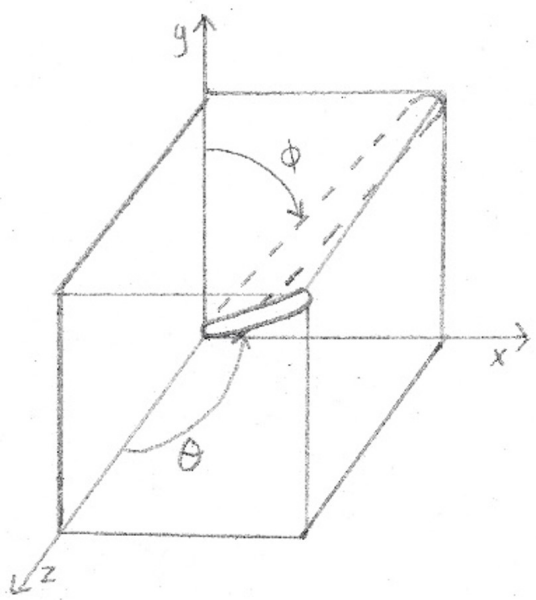

Figure 2: Schematic representation of a rod-like fiber in three-dimensional space, together with the definitions of the orientation angles ϕ and θ

The position of the fiber can also be described by using the orientation angles ϕ and θ. The angle ϕ describes the relative angle between the y-axis and the projection of the orientation vector on the xy-plane. And the angle θ describes the angle from the z-axis. These orientation angles are also shown in Figure 2. The relationship between the angles ϕ and θ and the xyz-coordinate system is

$$\vec{q} = \begin{pmatrix} \sin(\theta)\sin(\phi) \\ \sin(\theta)\cos(\phi) \\ \cos(\theta) \end{pmatrix} \tag{2}$$

where $\vec{q}$ is the orientation vector.

As mentioned before, polymer melts are subjected to shear flow and extensional flow. Describing these types of flows on a polymer melt with a rod-like fiber is done on a boundary box. On this boundary box, the flow

velocity profile corresponding with the flow is prescribed. For both simple shear flow and uniaxial extensional flow, it holds that the flow is incompressible, meaning the volume of this boundary box stays constant. The shear flow can be described in three unique planes, the xy-plane, the yz-plane, and the xz-plane. In this report, a shear flow will be in the xy-plane, this is shown in Figure 3. In shear flow, adjacent layers of fluid move parallel to each other with different velocities. The further away from the origin, the higher the velocity of the layer is going to be. The uniaxial extensional flow considered in this report takes place in the y-direction, this is shown in Figure 4. In uniaxial extension, the fluid is pulled from the top and the bottom. The dimensions in both the width and depth direction, z and x in this case, will decrease while the height direction, y, will increase. The resulting strain on the boundary box is a so-called Hencky strain [5].

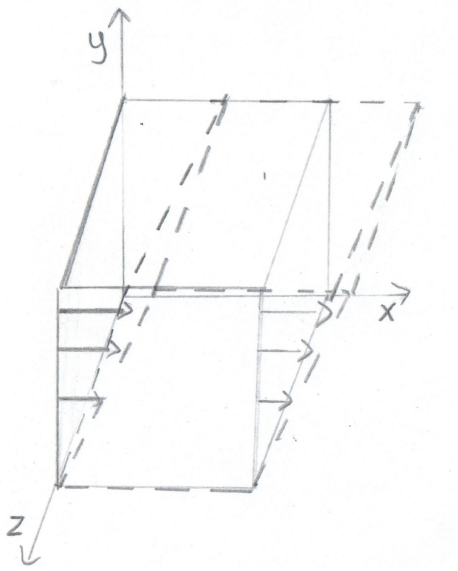

Figure 3: Schematic representation of shear flow

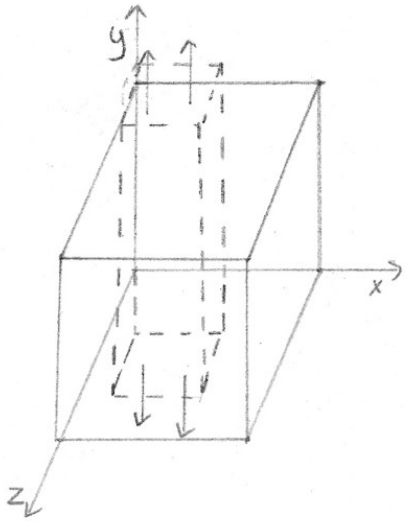

Figure 4: Schematic representation of extensional flow

The fiber is surrounded by fluid. The fluid flow is dependent on the fluid properties. An example of this is that water flows differently compared to honey. The fiber orientation kinetics might be different for different material parameters of the fluid. Therefore, the two main types of surrounding fluids considered in this report are a Newtonian fluid and a viscoelastic Giesekus fluid.

2.1 Newtonian fluid

A Newtonian fluid has a viscosity that is not dependent on shear rate. Typical examples of Newtonian fluids are water and air. The equations of motion describe the flow of a Newtonian fluid in steady-state [6] and are given by

$$\rho \frac{D\boldsymbol{v}}{Dt} = \nabla \cdot \boldsymbol{\sigma} + \rho \mathbf{b} + \mu \nabla^2 \boldsymbol{v}, \tag{3}$$

where ρ is the density, $\boldsymbol{v}$ is the velocity vector, $\boldsymbol{\sigma}$ is the stress tensor, $\boldsymbol{b}$ is the vector containing all body forces and μ is the dynamic viscosity. For incompressible flow, with low Reynolds numbers, no slip at the boundaries and body forces are negligible compared to the viscous forces Equation 3 can be further simplified

$$\nabla \cdot \boldsymbol{\sigma} = \mathbf{0}, \tag{4}$$

where $\mathbf{0}$ is the zero vector and $\boldsymbol{\sigma}$ is the stress tensor. This equation is an ordinary differential equation (ODE). The stress tensor can be decomposed as

$$\boldsymbol{\sigma} = -p\mathbf{I} + 2\eta_s D \tag{5}$$

with p is the pressure, $\boldsymbol{I}$ identity tensor, η_s is the Newtonian viscosity, and where D is the rate of deformation tensor defined as

$$\boldsymbol{D} = \frac{1}{2}(\nabla \boldsymbol{v} + (\nabla \boldsymbol{v})^T). \tag{6}$$

Besides the equation of motion, the continuity equation [6] also governs the flow. The continuity equation is an ordinary differential equation and reads as follows

$$\nabla \cdot \boldsymbol{v} = 0. \tag{7}$$

2.2 Viscoelastic Giesekus fluid

A Newtonian fluid is the most basic fluid model where the stress depends on the pressure, viscosity, and the rate of deformation tensor. A polymer melt shows behavior that a Newtonian fluid can not capture. That is why more complex models are required to describe the behavior of such polymer melts. Such polymer melts consist of long chains which can move relative to each other, but the chains are so long that they can form entanglements with each other. This results in more complex fluid behavior. This more complex behavior is known as viscoelastic behavior [7].

A model which can describe such viscoelastic behavior is the Giesekus model. The Giesekus model [8] defined as

$$\lambda \overset{\triangledown}{\boldsymbol{\tau}} + \boldsymbol{\tau} + \frac{\lambda\alpha}{\eta_p}\boldsymbol{\tau}^2 = 2\eta_p \boldsymbol{D} \tag{8}$$

where λ is the internal relaxation time, α is the non-linear dimensionless parameter, η_p is the viscosity, τ is the extra stress tensor and $\overset{\triangledown}{\boldsymbol{\tau}}$ is the time upper convected derivative of the extra stress tensor.

Similar to the Newtonian fluid, the equation of motion also describes the flow of this fluid. The difference between a Newtonian fluid and a viscoelastic Giesekus fluid comes in the decomposition of the stress tensor. The decomposition of the stress tensor for a Giesekus fluid is

$$\boldsymbol{\sigma} = -p\boldsymbol{I} + \boldsymbol{\tau} \tag{9}$$

where τ is the extra stress tensor as mentioned in Equation 8. For the Giesekus fluid, this extra stress tensor needs to be solved together with the ODE of the stress (Equation 4) and the continuity equation (Equation 7).

The viscoelastic Giesekus fluid has several important parameters. These parameters are α, λ and η_p. Furthermore, by means of scaling, it has been determined that α, Wi, and β are important parameters in Giesekus fluid analysis. The dependency of λ and η_p are found in the Wi and in β. This results in the following three important parameters: Wi, α, and β.

2.2.1 Wi

The Weissenberg number is a dimensionless number that looks at the velocity of the flow compared to its internal relaxation time. The Weissenberg number is defined as

$$Wi = \lambda\dot{\gamma} \tag{10}$$

where λ is the internal relaxation time and $\dot{\gamma}$ is the flow rate. When the Weissenberg number is much bigger than one, it can be seen as a fast deformation, in which there is not enough time for internal relaxation to occur. In fast deformation, the behavior of the fluid is the same as that of an ideal elastic solid. On the other hand, when the Weissenberg number is much smaller than one it can be seen as slow deformation, in this case, the internal structure rearranges to a lower stress state at every moment in time. In slow deformation, the fluid will behave the same as an ideal viscous fluid. The Weissenberg number tells if the fluid behavior is viscous or elastic.

2.2.2 α

The parameter α appears in the Giesekus model. This parameter is a non-linear parameter, its value lies between 0 and 0.5. Outside these bounds, this definition of the Giesekus model does not describe the polymer melt behavior. The α parameter is supposed to say something about the mobility of the fluid, which in practice dictates how fast shear thinning will take place [8]. Shear thinning is a non-Newtonian fluid behavior, where for increasing strain rate the viscosity goes down. In the Giesekus fluid model, the α parameter is in front of the $\boldsymbol{\tau}^2$ part of Equation 8. A high value of α will increase the effect of the $\boldsymbol{\tau}^2$ part of Equation 8. Likewise, a low value of α will decrease the influence of the second-order term.

2.2.3 β

β is a dimensionless number that compares the ratio between the viscosity of the solvent and the viscosity of the polymer.

$$\beta = \frac{\eta_s}{\eta_p + \eta_s} \tag{11}$$

Where η_s is the viscosity of the solvent and η_p is the viscosity of the polymers. A high value of β means that the total viscosity is dominated by the solvent, and a low value of β means that the total viscosity is dominated by the polymer. The solvent viscosity is usually the viscosity of a Newtonian fluid.

3 Jeffery orbits

The set of equations shown in Chapter 2 for the Newtonian fluid has an analytical solution. In order to obtain this analytical solution, several assumptions need to be made. The set of equations for the Newtonian fluid holds for any fluid and its corresponding geometry. For the analytical solution, the shape of the fiber is the shape of an ellipse. This is the first assumption to obtain the analytical solution. The problem definition showed a boundary box around the fiber. For the analytical solution, this boundary box is assumed to be infinitely big. This is the second assumption to obtain the analytical solution. The analytical solution is known for simple shear flow. Simple shear flow is when the velocity profile of shear flow looks like an upside down triangle. This is the shear flow as shown in Figure 3. Since for this analytical solution there is no boundary box, the shear field needs to be defined for simple shear. The shear field is

$$v^{\infty} = \dot{\gamma} y \vec{e_x} \tag{12}$$

where v^{∞} is the shear field, $\dot{\gamma}$ is the shear rate and y is the height from the xz-plane.

3.1 Analytical Jeffery solution

The analytical solution of the Jeffery Orbits [9] consists of two evolution equations. These evolution equations are

$$\dot{\phi} = \frac{\dot{\gamma}}{2} \frac{r_e^2 - 1}{r_e^2 + 1} \cos(2\phi) \tag{13}$$

$$\dot{\theta} = \frac{r_e^2 - 1}{r_e^2 + 1} \frac{\dot{\gamma}}{4} \sin(2\theta) \sin(2\phi). \tag{14}$$

Where $\dot{\gamma}$ is the shear rate, ϕ and θ are the orientation angles, and r_e is the aspect ratio, which is defined as

$$r_e = \frac{l}{d}. \tag{15}$$

Where l is the length of the ellipse and d is the diameter of the ellipse.

Using the following boundary conditions, the following equations are integrated with respect to time. The boundary condition is that $\phi = 0$ at $t = 0$. This angle ϕ is the tumbling angle in shear flow. This means that this angle will for a positive shear flow increase indefinitely. When integration with respect to time, an integration constant will appear. Together with the boundary conditions, this integration constant can be solved. In this case, the integration constant C [10] is equal to

$$C = \tan\left(\frac{\theta_0}{r_e (r_e^2 \cos^2(\phi_0) + \sin^2(\phi_0))^{-0.5}}\right) \tag{16}$$

where θ_0 and ϕ_0 are the initial angles of the fiber.

$$\tan(\theta) = \frac{C r_e}{\sqrt{r_e^2 \cos^2(\phi) + \sin^2(\phi)}} \tag{17}$$

$$\tan(\phi) = -r_e \tan\left(\frac{\dot{\gamma} t}{r_e + r_e^{-1}}\right) \tag{18}$$

Where C is the integration constant, r_e is the aspect ratio, $\dot{\gamma}$ is the shear rate and t is time. Equation 17 and Equation 18 are referred to as the analytical solution of the Jeffery's orbit [10].

3.2 Numerical integral solution

The evolution equations $\dot{\phi}$ and $\dot{\theta}$ given in Equation 13 and Equation 14 can be used to determine the values of ϕ and θ by means of numerical integration.

3.2.1 First order Euler integration scheme

The first method to determine the angle based on their first derivative is by means of Euler integration scheme. The first-order Euler integration scheme is a method to determine the value based on the value of the first derivative and time step.

$$\phi_{n+1} = \phi_n + \Delta t \dot{\phi_n} \tag{19}$$

Where ϕ_n is the angle at the current time step, ϕ_{n+1} is the angle at the new time step, Δt is the time step, and $\dot{\phi_n}$ is the angular velocity of ϕ at that time step. The same methodology can be applied for the angle θ.

3.2.2 Second order Adam-Bashford integration scheme

Another intergration method is the second-order Adam-Bashford integration scheme. The second-order Adam-Bashford integration scheme uses the time derivative of the first order of the last time step and the time step before that. This makes this integration scheme precise while remaining fast.

$$\phi_{n+1} = \phi_n + \Delta t(\frac{3}{2}\dot{\phi_n} - \frac{1}{2}\dot{\phi_{n-1}}) \tag{20}$$

Where ϕ_n is the current angle, ϕ_{n+1} is the new angle, Δt is the time step and $\dot{\phi_n}$ is the rotational speed of ϕ at that time step. And $\dot{\phi_{n-1}}$ is the rotational speed of the time step before the current one. The same methodology can be applied for the angle θ.

The Jeffery Orbits show an enclosed orbit, which the ellipsoidal-shaped fiber will follow. These orbits show the orientation of the ellipse during shear flow. An example of such an orbit is shown in Figure 5. The shear has been applied in the xy-plane.

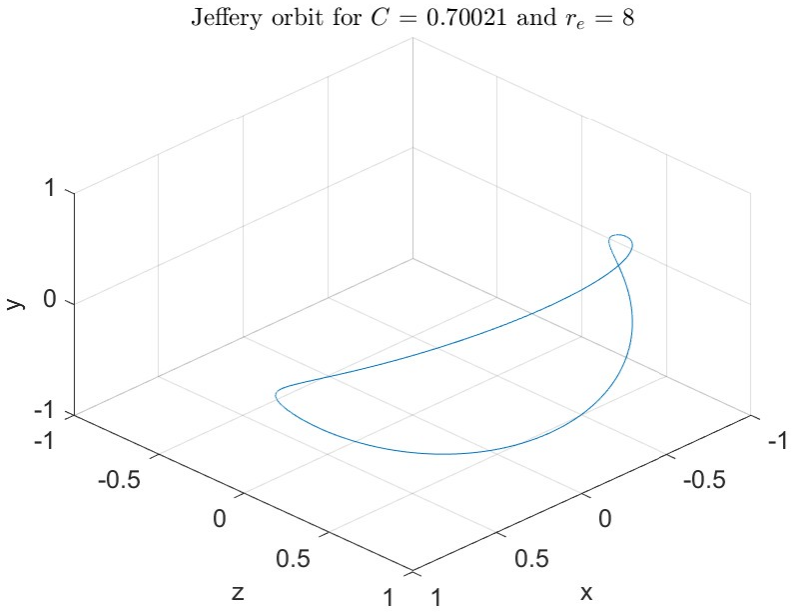

Figure 5: The Jeffery Orbit for a fiber with aspect ratio of 8 and an integration constant equal to 0.7

4 FEM theory

For viscoelastic fluid such as the Giesekus fluid as described in Chapter 2.2 there is no analytical solution. For this reason, another method needs to be used to obtain a solution to the flow problem. A method to obtain such a solution for fiber kinetics is using FEM software. The in-house – FINITE ELEMENT METHOD TFEM, will be used to obtain the orientation of a single fiber as a function of time. The remainder of this chapter will discuss some fundamental theories about FEM.

In the Finite Element Method, the domain is divided into many small elements, which is called the mesh. In Figure 6 the dashed lines represent the smaller elements of the big box. The more elements used, the more accurate the result will be of the simulation. However, the more elements used, the more time the computations will take.

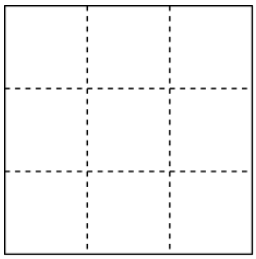

Figure 6: Schematic representation of a meshed cube using squared elements

For each of these meshelements, the set of ODEs (Equation 4, Equation 8 and Equation 7) needs to be solved. For the problem described in chapter 2.1, there remain three unknown fields. Namely, the velocity field, the pressure field and the stress field. All these fields depends on the spatial position and time. For the pressure and the stress field, this is done linearly, which is visibly shown by the blue circles at the corner pieces in Figure 7. The red squares represent a quadratic linearization, which is used for velocity.

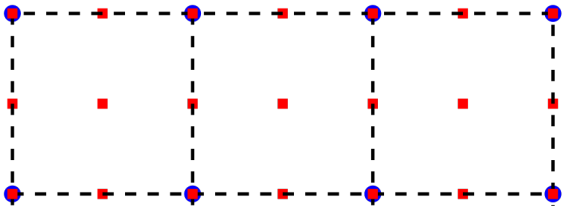

Figure 7: Schematic representation of the different discretization methods for squared elements. The linear discretization (blue circles) and quadratic discretization (red squares) are shown for three consecutive elements

The FEM method used in TFEM is Discrete Elastic Viscous Split Stress-G/Streamline Upwind Petrov Galerkin formulation [11–13] together representing the conformation tensor by a logarithmic expression [14, 15]. To stabilize the domain, a Newtonian solvent is assumed. This means that the stress tensor consist out of three parts

$$\boldsymbol{\sigma} = -p\boldsymbol{I} + 2\eta_s \boldsymbol{D} + \boldsymbol{\tau}. \tag{21}$$

Here η_s is the viscosity of the Newtonian solvent. The stress tensor has a pressure part, a Newtonian viscosity contribution and a extra viscous stress part. To be able to compare the values of the viscous viscosity and the Newtonian viscosity β is used as defined in Equation 11. The bounding box is simulated as being periodic on all sides. This will result in a tri periodic box with boundary conditions. Instead of simulating a bunch of fibers, a single fiber is being simulated and is assumed to be spaced homogeneous over the whole domain. When taking a significantly big size of the bounding box, the influence of the surrounding fibers will not be dominating the movement of the single fiber.

From the TFEM package, the angular velocities are obtained. These angular velocities need to be integrated using an integration scheme as discussed in Chapter 3.2 to obtain the orientation angles. With these resulting orientation angles, the orientation vector can be computed and saved for every time step.

5 Validation

To establish confidence in the TFEM simulations, the results will be compared to the analytical solution for Newtonian flows. The analytical solution is shown in Chapter 3.1 and the numerical integral solution is shown in Chapter 3.2. For the comparison with TFEM two types of convergence tests have been performed, namely time convergence and mesh convergence.

5.1 Influence of integration schemes compared to analytical solution

During the TFEM simulation, both the mesh size and the time step contribute to the error. To remove the influence of the mesh effect, the time convergence is done between the numerical integral solution, in which the time step error occurs, and the analytical solution which does not have a time step error. The comparison below is for the Jeffery Orbits and not the TFEM simulations.

Both the numerical integration scheme and the analytical solution are computed using MatLab. The code for the analytical solution can be seen in Appendix B. The code for the integral solution can be seen in Appendix C. The first step in time in the Adam-Bashford scheme is the Euler scheme. To check for the error, the mean of the absolute distance between the direction vectors at any given time is looked at

$$e = \sqrt{(x_i - x_a)^2 + (y_i - y_a)^2 + (z_i - z_a)^2}. \tag{22}$$

The index of i stands for the integration scheme and the index of a stands for the analytical solution. For both integration schemes Euler (first order) and Adam-Bashford (second order) the difference is computed for a range of different time steps shown in Figure 8.

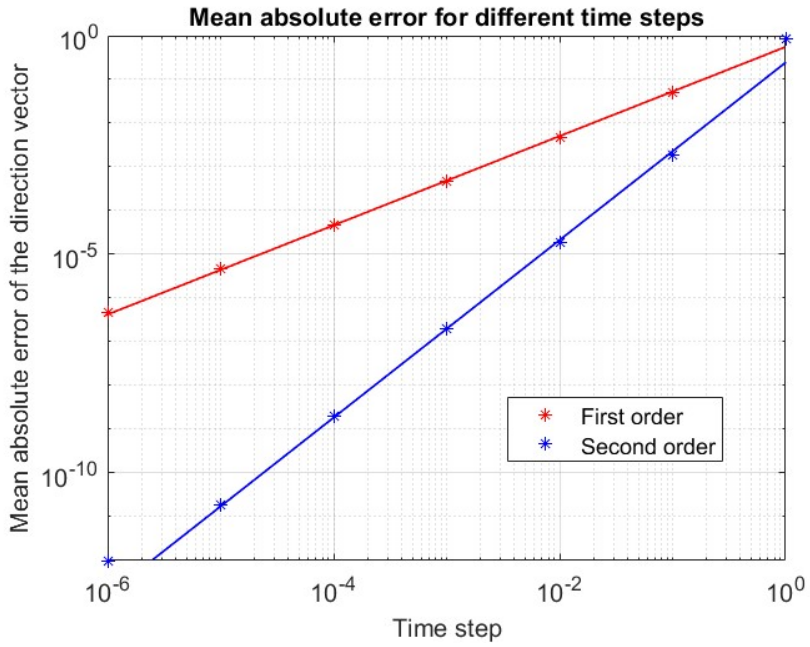

Figure 8: Graphical representation of the error between numerical and analytical solution for decreasing timesteps (r_e = 2)

For both integration schemes, the error decreases when taking a smaller time step. However, the main difference is that for the first-order integration scheme (Euler) the reduction for each decade of a time step is also a decade for the error, while for the second-order integration scheme (Adam-Bashford) a decade reduction for the time step means a reduction of two decades for the error. For the simulations, it is desirable to have a larger time step while keeping the error low. For this reason, the second-order Adam-Bashford integration scheme with a time step of 0.01 will be used in the TFEM simulations. By doing this, the error due to the time step is below 10^{-4} while still having the benefits of using a larger time step.

5.2 Influence of box size and mesh sizes

After obtaining the effect of the error caused by the time step, the effect of the simulation parameters needs to be done with a mesh convergence study. For the simulations using the TFEM package, two main parameters were identified to have a big influence on the error. Firstly, the box size since the simulation assumes a tri-periodic cube while the Jeffery Orbits is defined for a particle in an infinitely big space and the mesh sizes. The code makes a difference between the mesh of the fiber and the mesh of the surrounding box. The finer the meshes, the more precise the calculations will be. To determine the best set of parameters, several simulations were done with different parameters.

To compare the analytical solution with the simulations, a single fiber has been simulated perpendicular to the shearing direction. The angular velocities after solving for the first time are compared. By doing this, the error caused by the time step is removed. The fiber has a radius of 0.11 in the simulations and an aspect ratio of 4. For both cases, the angular velocity has been determined and compared by using

$$e = |\dot{\vec{q}}_a - \omega_s|. \tag{23}$$

The $\dot{\vec{q}}_a$ is derived from Equation 2, the full derivation can be seen in Appendix A and ω_s is obtained from the simulations. For this perpendicular case, the only significant rotation takes place in a single direction. That is why only a comparison has been made between the main rotational direction.

5.2.1 Influence box size

For this comparison, the mesh size of the fiber has been kept constant (0.05) to check the influence of the other two parameters. After comparing the angular velocity computed at the first time step and the analytical solution for the same angular velocity, a comparison is made. The error is computed as defined in equation 23. For different box sizes, the error has been determined, this is shown in Figure 9.

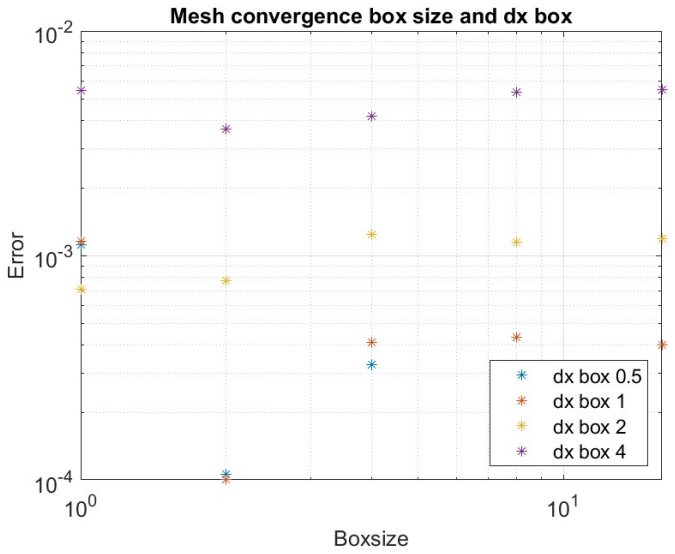

Figure 9: Graphical representation of the error in the mesh convergence between the box size and the coarse mesh

Figure 9 shows that once a box size of 4 is used, increasing the box size does not significantly change the error anymore. This means that from that moment on, the error is dominated by other parameters, such as the fineness of the mesh sizes.

5.2.2 Influence mesh sizes

Equivalent to determining the right box size, one of the parameters has been kept constant. In this case, the box size is set to 4x4x4. A comparison has been made between the angular velocity obtained from the simulations and the angular velocity obtained from the analytical solution. The error is computed as shown in Equation 23.

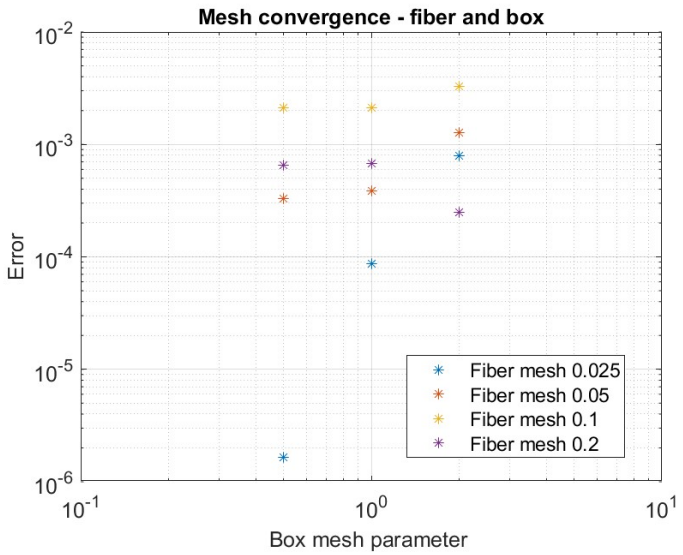

Figure 10: Graphical representation of the error in the mesh convergence for the fine fiber mesh and the coarse box mesh

Figure 10 shows that when the fiber mesh is set to 0.05 and the coarse box mesh is set to 2 the error is significantly small. This will not disturb the simulation results while still reducing the simulation time significantly.

In FEM methods, the error heavily depends on the number of elements that are contained by the mesh. The error compared to the number of elements is shown in Figure 11. In this figure, the general trend has a -3 slope, with having on the x-axis the cubic root of the number of elements and the error on a log scale.

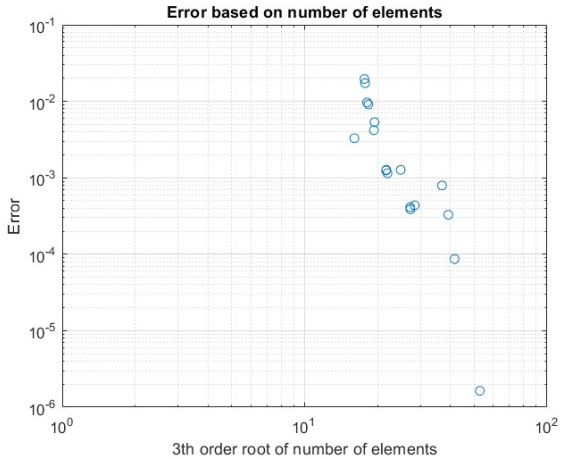

Figure 11: Graphical representation of the error based on the number of elements

To conclude this part of the validation, the following settings will be used for the TFEM software. The time step is going to be 0.01 with a second-order Adam-Bashford integration scheme to obtain the orientation angles. The box size is at minimum 4x4x4 for a fiber with a length of 0.11. The fine mesh of the fiber is set to 0.05 and for the coarse box mesh the size is set to 2.

5.3 Difference between ellipsoidal shaped fiber and spherocylindrical fiber

The Jeffery Orbits are known for an ellipse. The shape of hard fiber is not the shape of an ellipse, but rather of a long rod with rounded edges. For this reason, a cylinder with hemispheres at the ends can be used to model the fiber. This shape is called a spherocylinder. Another problem with using an elipsoidal fiber is that

for larger aspect ratios, the shape of the ellipsoidal fiber gives rise to numerical issues due to the sharp point that will be at the endpoints. In the simulations, the radius and aspect ratio has been set to be constant for both shapes, meaning that the volume will not be exactly the same for the two shapes.

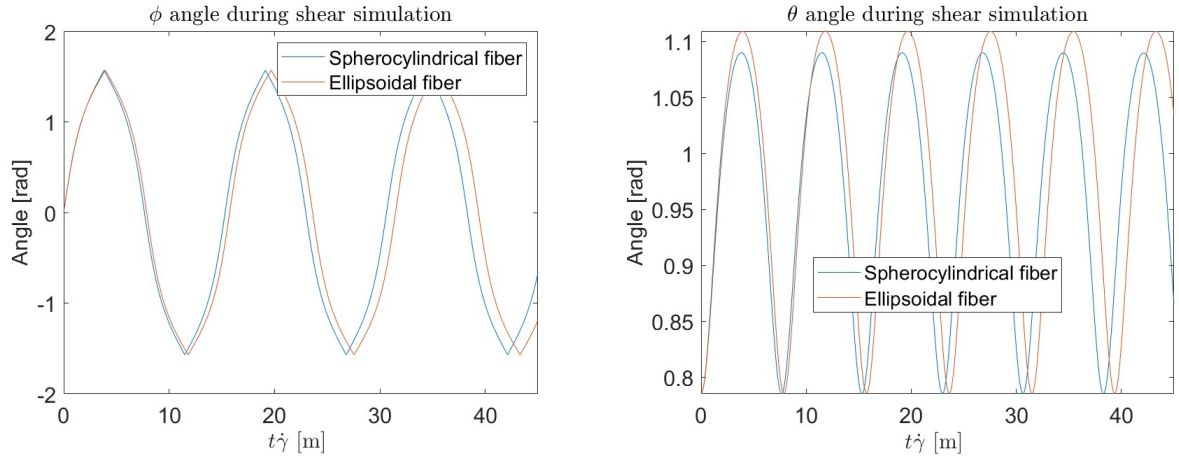

(a) The angle ϕ as function of strain during a shear simulation

(b) The angle θ as a function of strain during a shear simulation

Figure 12: Difference between an ellipsoidal-shaped fiber and a spherocylindrical-shaped fiber

As Figure 12a shows, the angular velocity of the spherocylindrical fiber is slightly larger compared to the ellipsoidal shaped fiber. Figure 12b shows the angle θ as a function of shear rate. The amplitude of this angle is larger for an ellipsoidal shaped fiber compared to a spherocylindrical shaped fiber. This variation in the angle θ will cause for a different shaped orbit. The most significant change can be seen in the yz-plane, which is shown in Figure 13. Here, it is visible that the orbit of the ellipsoidal shaped fiber is bigger than the orbit of the spherocylindrical shaped fiber.

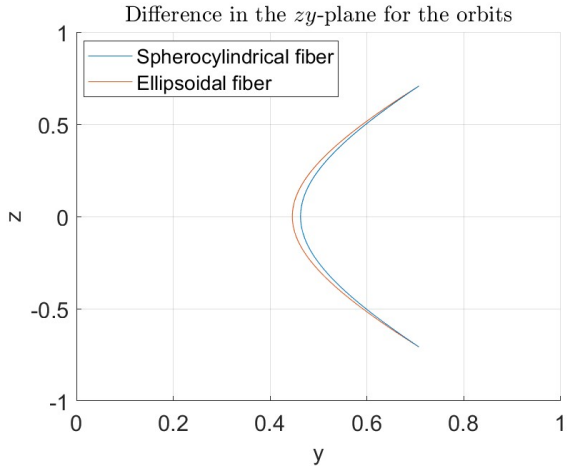

Figure 13: zy-plane indicating the difference in orbits between the spherocylindrical fiber and the ellipsoidal shaped fiber

6 Results

In this chapter, the results of the TFEM simulations are shown for the problem as discussed in Chapter 2. The fiber orientation is investigated for shear and uniaxial extensional flow. The end conditions for the simulations have been set for shear flow to be at a time of 45 seconds, and for extensional flow until a Hencky strain of 30 has been reached. The shear direction in the simulations is the xz-plane. The extension direction in the simulations is the z-direction. The influence of α, Weissenberg number, and β are all studied as they have been identified in Chapter 2.2 as the most important parameters. The study is performed considering a fiber aspect ratio of 2 and a fiber with an aspect ratio of 8. On top of that, three different initial values of orientation angle θ: 1, 45 and 89 degrees have been studied. The initial value for the orientation angle ϕ is always 0. This means that the fiber initially is in the yz-plane. The initial orientations of the fiber are shown in Figure 14. For visibility reasons, the 1-degree angle is shown as a 3-degree angle and the 89-degree angle is shown as an 86-degree angle.

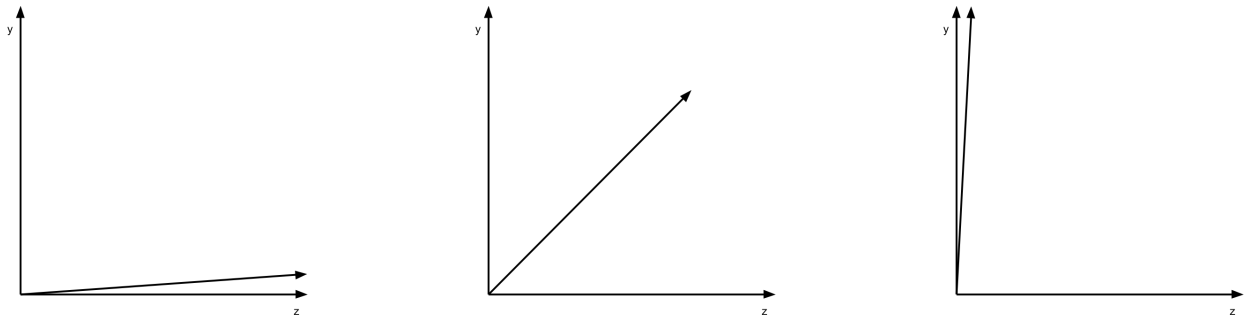

(a) Orientation of the fiber when θ is equal to 3 degrees

(b) Orientation of the fiber when θ is equal to 45 degrees

(c) Orientation of the fiber when θ is equal to 86 degrees

Figure 14: The three different starting positions for the fiber used in the simulations

6.1 Influence of α

To investigate the influence of α other two parameters, have been set to a constant value (β = 0.01 & Wi = 1), while the value of the α parameter has been varied. For α the values for the variation are 0.49, 0.05 and 0.005. In shear flow, the influence of α will be shown by means of three figures, one figure will show the orientation of the fiber in a three-dimensional space, the other two figures will show the orientation angles ϕ and θ as a function of strain. These three figures combined give a good overview of time effects as well as the spatial effects that take place. The influence of α in shear flow with an aspect ratio of 2 can be seen in Figures 15, 16 and 17.

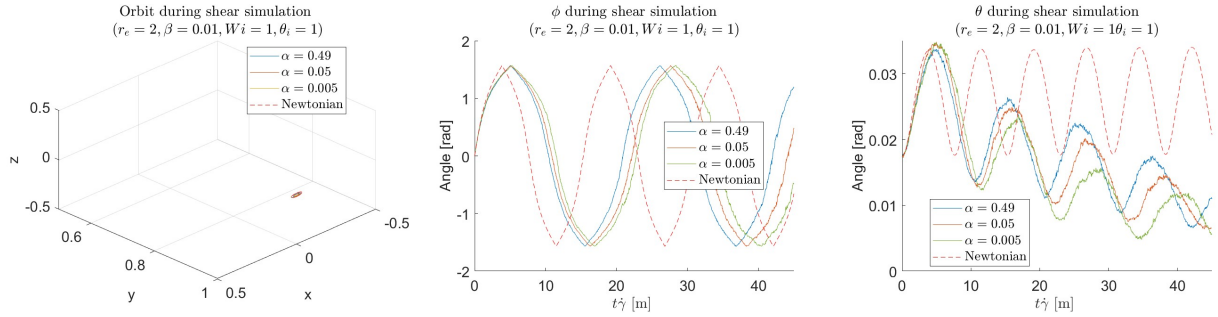

(a) Orientation of the fiber

(b) The angle ϕ as a function of strain

(c) The angle θ as a function of strain

Figure 15: Influence of α for an initial orientation of θ = 1 and an aspect ratio of 2

Figure 15a shows the orientation of the fiber in three-dimensional space. Figure 15b shows the tumbling angle ϕ as a function of strain. The higher the value of α, the higher the angular velocity is. Figure 15c shows the angle θ as a function of strain. All three viscoelastic simulations show a drift towards the zero value in z-direction. The higher the value of α is, the slower this drift goes.

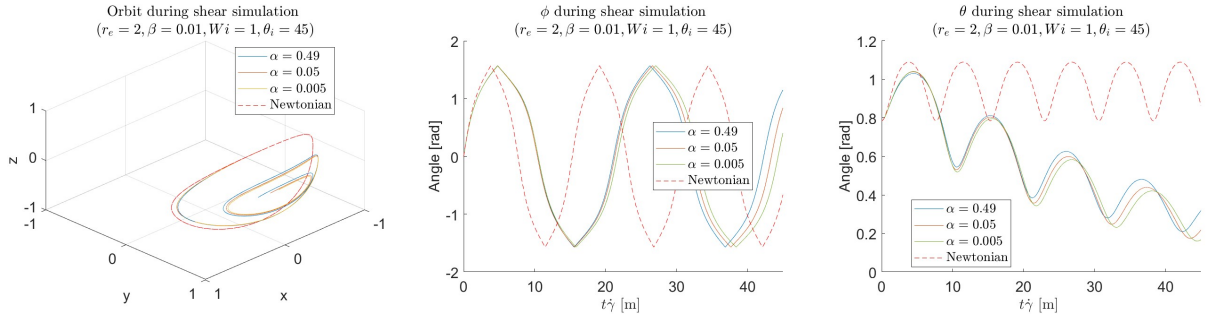

(a) Orientation of the fiber (b) The angle ϕ as a function of strain (c) The angle θ as a function of strain

Figure 16: Influence of α for an initial orientation of θ = 45 and an aspect ratio of 2

Figure 16a shows the orientation of the fiber in three-dimensional space. For the three viscoelastic simulations, a spiral pattern is visible. Figure 16b shows the tumbling angle ϕ as a function of strain. Figure 16c shows the angle θ as a function of strain. All three viscoelastic simulations show a drift towards the zero value of the z-direction, and the orientation is moving towards the x-direction. This effect is not depending on the value α.

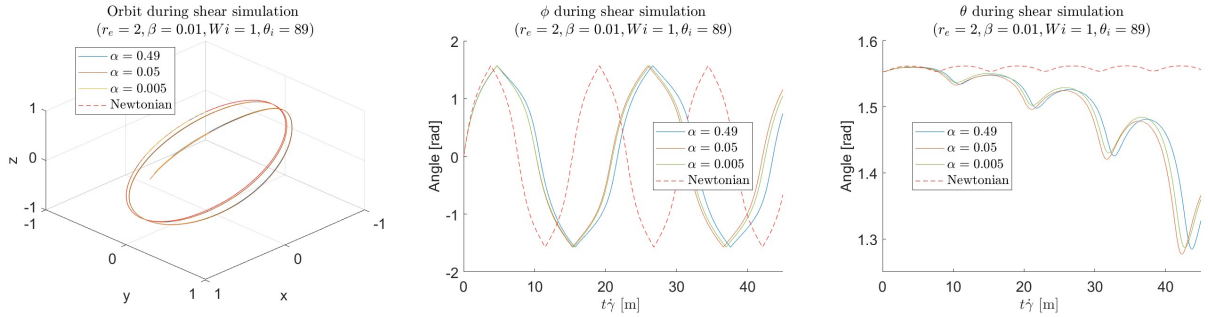

(a) Orientation of the fiber (b) The angle ϕ as a function of strain (c) The angle θ as a function of strain

Figure 17: Influence of α for an initial orientation of θ = 89 and an aspect ratio of 2

Figure 17a shows the orientation of the fiber in three-dimensional space. Figure 17b shows the tumbling angle ϕ as a function of strain. Figure 17c shows the angle θ as a function of strain. The angle of θ decreases over strain for all three viscoelastic simulations. This indicated that this effect is not dependent on α.

A realistic hard fiber has a higher aspect ratio than 2. For this reason, the same set of simulations has been performed using a higher fiber aspect ratio equal to 8. The influence of α in shear flow for a fiber aspect ratio of 8 can be seen in Figures 18, 19 and 20.

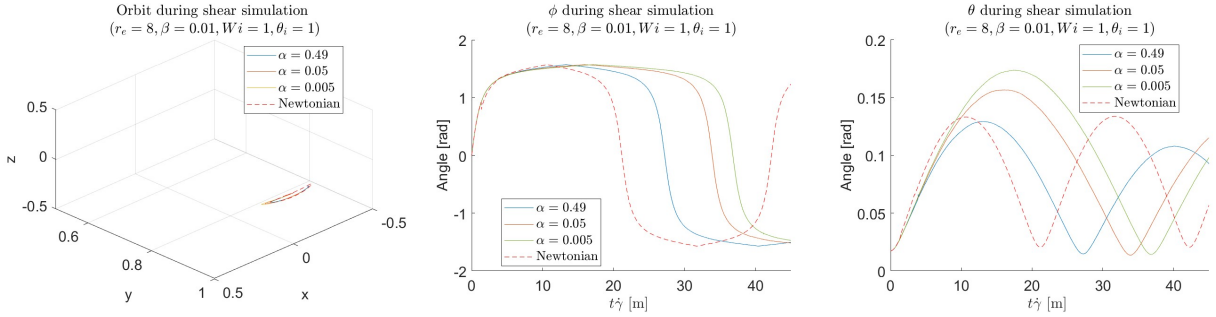

(a) Orientation of the fiber (b) The angle ϕ as a function of strain (c) The angle θ as a function of strain

Figure 18: Influence of α for an initial orientation of θ = 1 and an aspect ratio of 8

Figure 18a shows the three-dimensional orientation of the fiber. Figure 18b shows the tumbling angle ϕ. The angular velocity of angle ϕ at the positions where the fiber aligns with the shear flow direction is much lower compared to the rest of the orientations. The higher the value of α is, the lesser this effect is. Figure 18c shows the angle θ as a function of strain. The amplitude of the angle θ decreases for a higher value of α. Besides that, the higher the value of α is, the higher the angular velocity of the angle θ is.

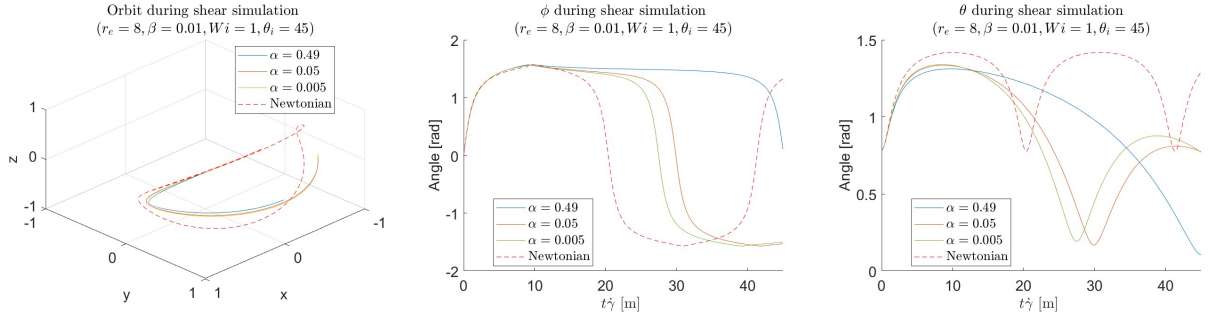

(a) Orientation of the fiber (b) The angle ϕ as a function of strain (c) The angle θ as a function of strain

Figure 19: Influence of α for an initial orientation of θ = 45 and an aspect ratio of 8

Figure 19a shows the orientation of the fiber in three-dimensional space. Figure 19b shows the tumbling angle ϕ. For this tumbling angle ϕ, the angular velocity around the shear flow direction is much lower than for the other orientation directions of ϕ. This effect in angular velocity is higher for higher values of α. Figure 19c shows the angle θ decreasing over strain for all three viscoelastic simulations. For higher values of α, this effect goes faster.

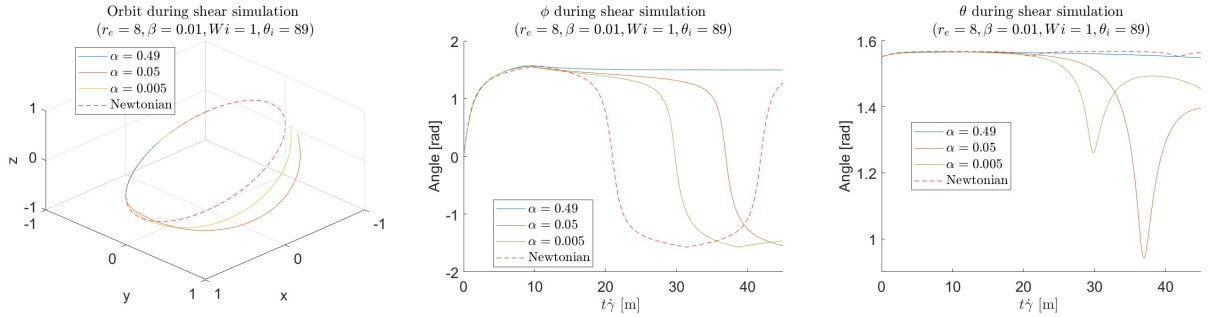

(a) Orientation of the fiber (b) The angle ϕ as a function of strain (c) The angle θ as a function of strain

Figure 20: Influence of α for an initial orientation of θ = 89 and an aspect ratio of 8

Figure 20a shows the orientation of the fiber in three-dimensional space. Figure 20b shows the tumbling angle ϕ. Figure 20c shows the orientation angle θ as function of strain. The angular velocity of the angle ϕ goes faster for lower values of α. The higher α is, the longer the fiber stays aligned with the shear direction.

Uniaxial extensional flow

Now, simulations are performed to investigate the influence of the parameter α on the fiber kinetics for uniaxial extensional flow. In uniaxial extension, the angle ϕ remains constant and is thus therefore not considered in the analysis. Likewise, the three-dimensional orientation in extensional flow will, for the used initial angles of θ always show the fiber aligning with the flow direction. For this reason, this figure is not considered in the results. The initial angles of θ which are relevant for uniaxial extension are a starting angle of 1 degree and 45 degrees. The initial angle for ϕ still remains zero degrees. The influence of α in extensional flow for a fiber with an aspect ratio of 2 can be seen in Figure 21 and in Figure 22 with a fiber aspect ratio of 8.

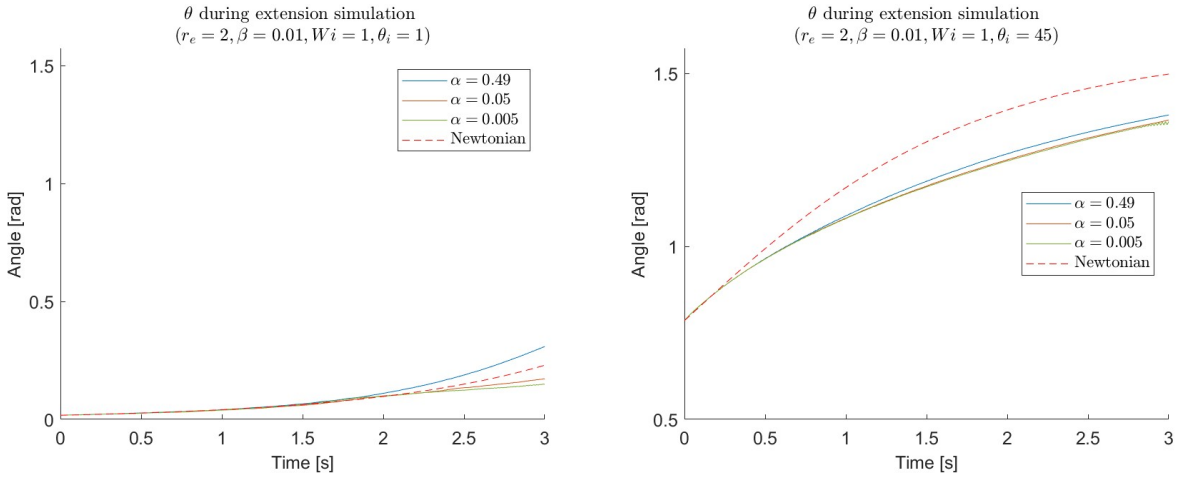

(a) The angle θ with initial angle θ equal to 1 degree (b) The angle θ with initial angle θ equal to 45 degrees

Figure 21: Influence of α in extensional flow for a fiber with aspect ratio 2

Figure 21a shows the angle θ as a function of strain when the fiber was initially orientated 1 degree for the angle θ. The higher the value of α, the higher the angular velocity is. Figure 21b shows the angle θ as a function of strain when the fiber was initially orientated to be 45 degrees for the angle θ. This figure shows that all three viscoelastic simulations have a lower angular velocity compared to the angular velocity the fiber would have in a Newtonian fluid. This effect is not dependent on the value of α.

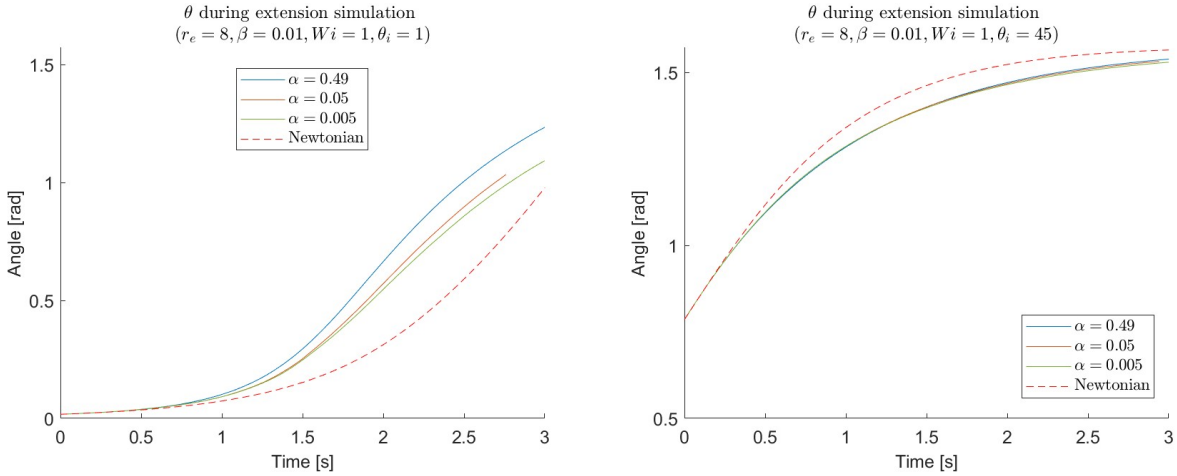

(a) The angle θ with initial angle θ equal to 1 degree (b) The angle θ with initial angle θ equal to 45 degrees

Figure 22: Influence of α in extensional flow for a fiber with aspect ratio 8

Figure 22a shows the angle θ as a function of strain when the fiber was initially orientated 1 degree in the direction of the angle θ. The three viscoelastic simulations show a higher angular velocity than the angular velocity for the Newtonian fluid simulation. The angular velocity is at the beginning of the experiment lower than the angular velocity at the end of the experiment. This change in angular velocity results in a curvature that initially increases slowly, in the middle section the curvature is steeper and in the end section, the curvature becomes less steep. The angular velocity is higher for higher values of α. Figure 22b shows the angle θ as a function of strain when the fiber was initially orientated 45 degrees in the direction of the angle θ. All three viscoelastic simulations show a lower angular velocity than the angular velocity of the Newtonian fluid. In this simulation, there is no influence of the parameter α.

6.2 Influence of Weissenberg number

This section of the report will focus on the influence of the Weissenberg number on the kinetics of the fiber. To isolate the influence of the Weissenberg number (Wi) the parameters α and β are kept at the constant values of 0.05 and 0.01 respectfully. For the Weissenberg number, the values of 0.1, 1, and 10 have been studied. The influence of the Weissenberg number is for shear flow with a fiber aspect ratio of 2 shown in Figure 23, Figure 24 and Figure 25.

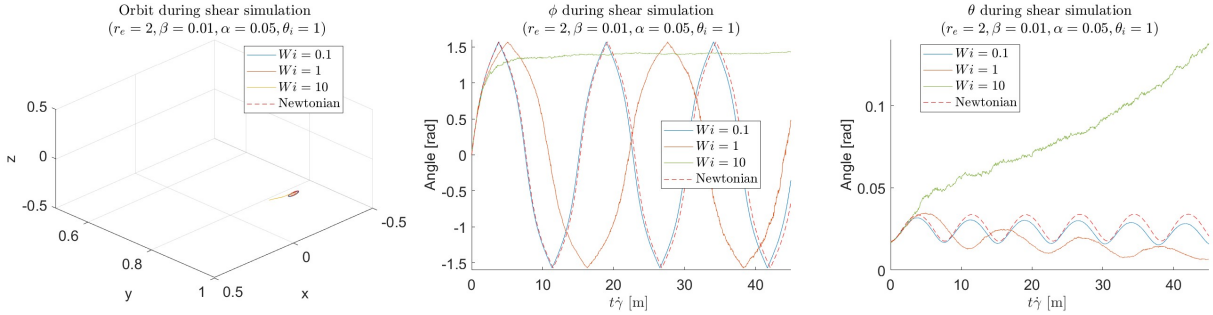

(a) Orientation of the fiber (b) The angle ϕ as a function of strain (c) The angle θ as a function of strain

Figure 23: Influence of the Weissenberg number for an initial orientation of θ = 1 and an aspect ratio of 2

Figure 23a shows the orientation of the fiber in three-dimensional space. Figure 23b shows the tumbling angle ϕ during the shear simulation. For a Weissenberg number equal to 0.1 this tumbling angle ϕ has a similar angular velocity as for the Newtonian fluid. For a Weissenberg number equal to 1 the angular velocity is higher. For a Weissenberg number of 10 the angle ϕ seems to remain more or less constant. Figure 23c shows the angle θ during the shear simulations. When the Weissenberg number is equal to 1 or 0.1 drifting takes place, while for a Weissenberg number equal to 10 the θ angle increases over strain.

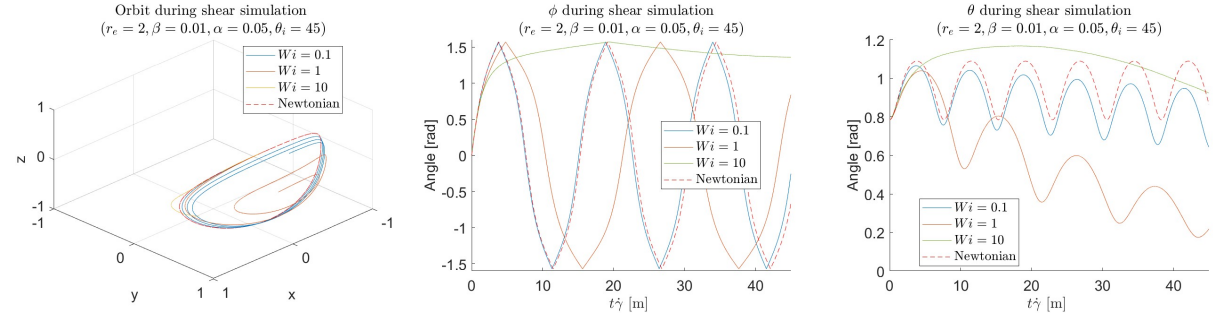

(a) Orientation of the fiber (b) The angle ϕ as a function of strain (c) The angle θ as a function of strain

Figure 24: Influence of the Weissenberg number for an initial orientation of θ = 45 and an aspect ratio of 2

Figure 24a shows the orientation of the fiber in three-dimensional space for different Weissenberg numbers. A Weissenberg number equal to 1 results in a spiraling pattern for the orientation of the fiber. For a lower Weissenberg number, this spiraling is happening at an angular velocity, resulting in more spirals before reaching alignment with the x-axis. For a Weissenberg number equal to 10 this spiraling does not happen, rather it moves very slowly toward the y-axis. In Figure 24b and Figure 24c the angles ϕ and θ are shown as a function of strain.

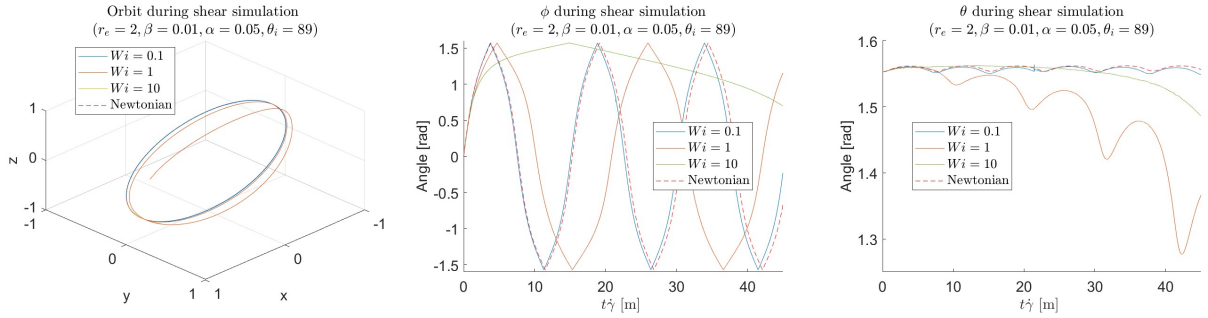

(a) Orientation of the fiber (b) The angle ϕ as a function of strain (c) The angle θ as a function of strain

Figure 25: Influence of the Weissenberg number for an initial orientation of $\theta = 89$ and an aspect ratio of 2

Figure 25a shows the orientation of the fiber in three-dimensional space. Figure 25b and Figure 25c show the angles ϕ and θ respectfully as a function of strain. For a Weissenberg number equal to 0.1 the movement of the fiber is similar to the Newtonian fluid. For a Weissenberg number equal to 1, the fiber slowly spirals down toward the x-axis. For a Weissenberg number equal to 10, the fiber orientates very slowly towards the y-axis.

A realistic hard fiber has a higher fiber aspect ratio than 2. For this reason, the same set of simulations has been performed using a higher fiber aspect ratio equal to 8. The influence of the Weissenberg number in shear flow for the fiber with an aspect ratio of 8 can be seen in Figure 26, Figure 27 and Figure 28.

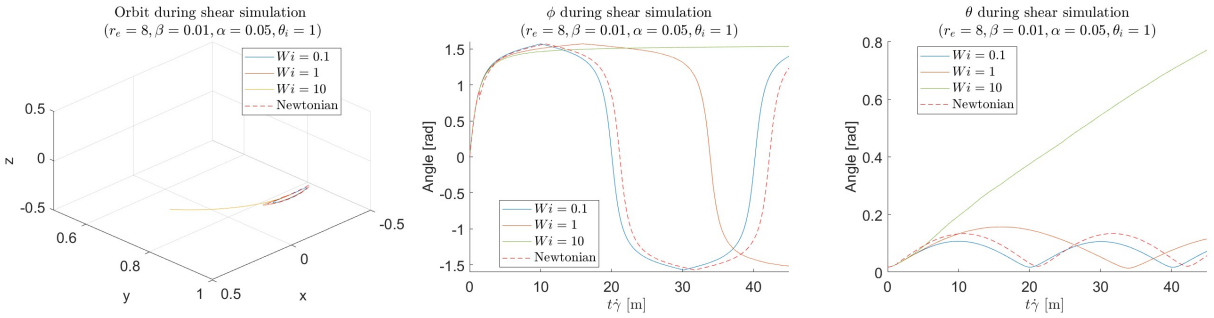

(a) Orientation of the fiber (b) The angle ϕ as a function of strain (c) The angle θ as a function of strain

Figure 26: Influence of the Weissenberg number for an initial orientation of $\theta = 1$ and an aspect ratio of 8

Figure 26a shows the orientation of the fiber in three-dimensional space for the different Weissenberg numbers. For a Weissenberg number equal to 10, the fiber slowly rotates towards the y-direction. Figure 26b shows the angle ϕ for the different Weissenberg numbers. A lower Weissenberg number results in faster angular velocities. Furthermore, for a Weissenberg number equal to 1 the fiber has a lower angular velocity around the shear flow direction, this is not the case for the Weissenberg number equal to 0.1 which has a similar speed as for the Newtonian fluid. Figure 26c shows the orientation angle θ as a function of strain for the different Weissenberg numbers. The higher the Weissenberg number is, the higher the peak value of θ is.

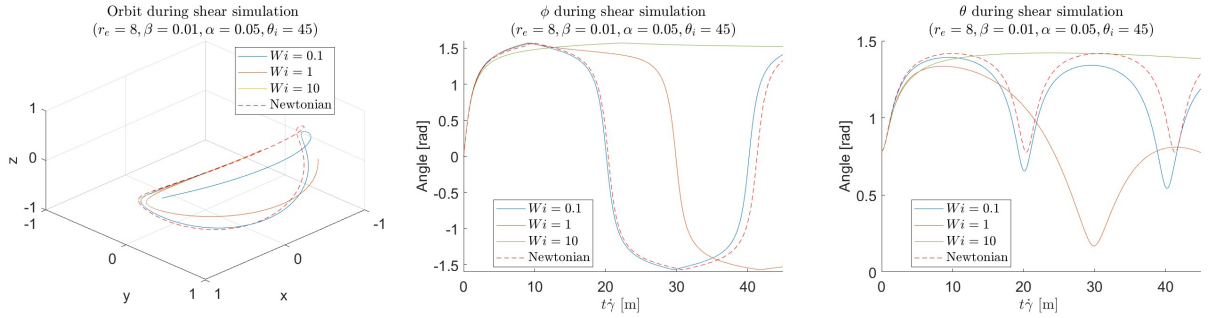

(a) Orientation of the fiber (b) The angle ϕ as a function of strain (c) The angle θ as a function of strain

Figure 27: Influence of the Weissenberg number for an initial orientation of θ = 45 and an aspect ratio of 8

Figure 27a shows the orientation of the fiber in three-dimensional space for the different Weissenberg numbers. Figure 27b shows the angle ϕ as a function of strain for the different Weissenberg numbers. Figure 27c shows the angle θ as a function of strain for the different Weissenberg numbers. A lower Weissenberg number results in faster angular velocities. Furthermore, for a Weissenberg number equal to 1 the fiber has a lower angular velocity around the shear flow direction, for the Weissenberg number equal to 0.1 the angular velocity is similar to the angular velocity of the Newtonian fluid. For a Weissenberg number equal to 10, the fiber slowly rotates toward the y-axis.

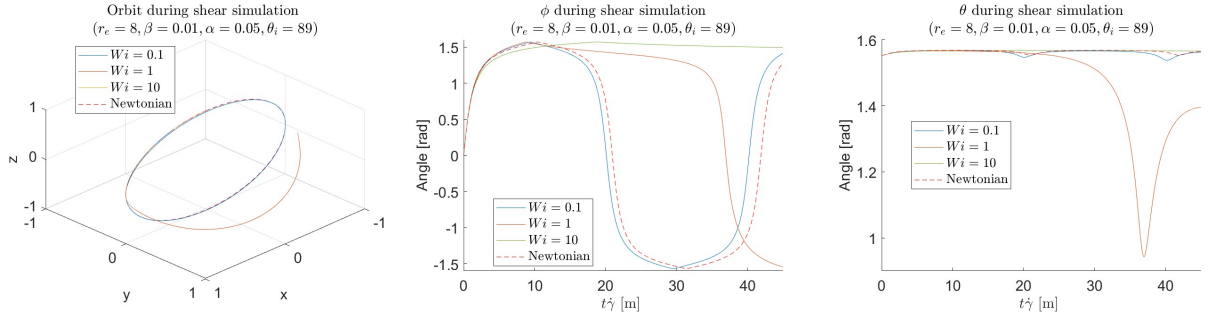

(a) Orientation of the fiber (b) The angle ϕ as a function of strain (c) The angle θ as a function of strain

Figure 28: Influence of the Weissenberg number for an initial orientation of θ = 89 and an aspect ratio of 8

Figure 28a shows the orientation of the fiber in three-dimensional space for the different Weissenberg numbers. Figure 28b shows the angle ϕ as a function of strain for the different Weissenberg numbers. Figure 28c shows the angle θ as a function of strain for the different Weissenberg numbers. For a Weissenberg number equal to 0.1, the angular velocity is faster than for the Newtonian fluid. For a Weissenberg number equal to 1 the fiber has a lower angular velocity around the shear flow direction. For a Weissenberg number equal to 10, the fiber aligns perpendicular to the flow direction.

Uniaxial extensional flow

Now, simulations are performed to investigate the influence of the Weissenberg number on the fiber kinetics for uniaxial extensional flow. In uniaxial extension, the angle ϕ remains constant and is thus therefore not considered in the analysis. Likewise, the three-dimensional orientation in extensional flow will, for the used initial angles of θ, always show the fiber aligning with the flow direction. For this reason, this figure is not considered in the results. The initial angles of θ which are relevant for uniaxial extension are a starting angle of 1 degree and 45 degrees. The initial angle for ϕ still remains zero degrees. The influence of the Weissenberg number in extensional flow for a fiber with an aspect ratio of 2 can be seen in Figure 29 and in Figure 30 with a fiber aspect ratio of 8.

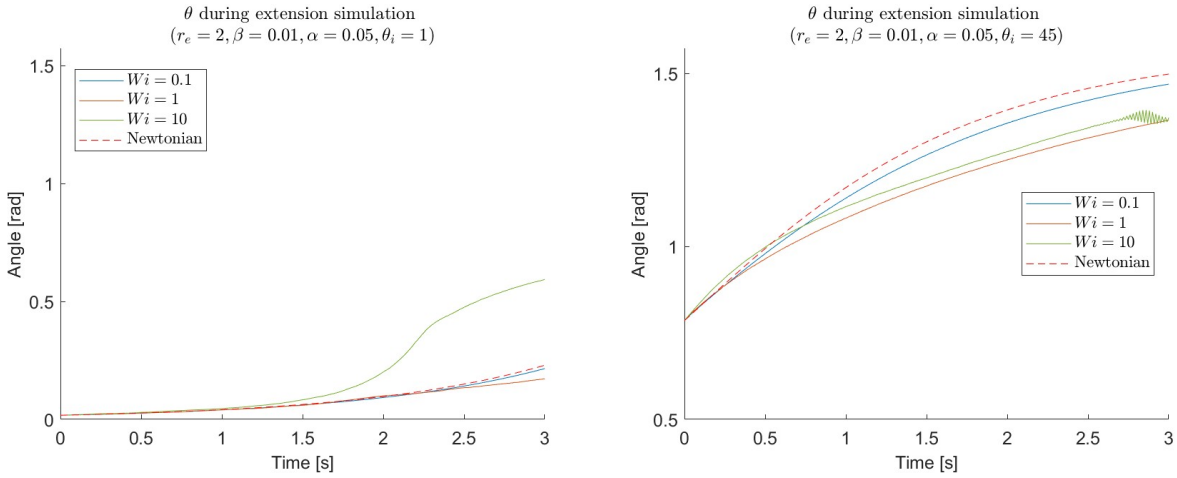

(a) The angle θ with initial angle θ equal to 1 degree (b) The angle θ with initial angle θ equal to 45 degrees

Figure 29: Influence of the Weissenberg number in extensional flow for a fiber with aspect ratio 2

Figure 29a shows the angle θ during the extension experiment with an initial orientation of 1 degree. For a Weissenberg number equal to 10 the angular velocity is higher up to a certain strain value, after which the angular velocity will decrease again. For the other two values of the Weissenberg number, there is no dependency. Figure 29b shows the θ angle during the extension experiment with an initial orientation of 45 degrees. For a Weissenberg number equal to 10 the initial angular velocity is faster and will decrease over strain. A Weissenberg number of 0.1 has a higher angular velocity than when the Weissenberg number is equal to 1.

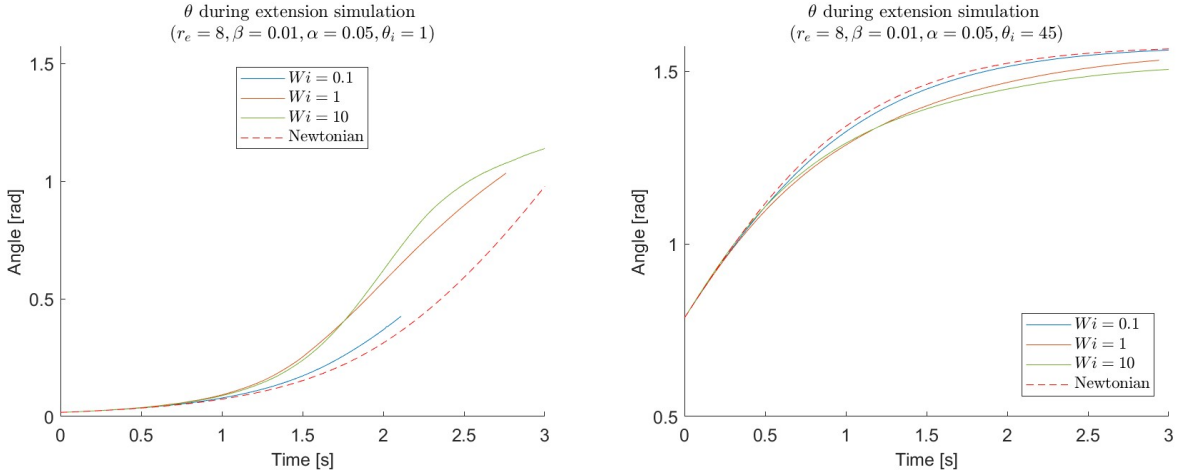

(a) The angle θ with initial angle θ equal to 1 degree (b) The angle θ with initial angle θ equal to 45 degrees

Figure 30: Influence of the Weissenberg number in extensional flow for a fiber with aspect ratio 8

Figure 30a shows the angle θ as a function of strain for the extensional simulation with a fiber aspect ratio equal to 8 and with the initial orientation of 1 degree. Both for a Weissenberg number of 1 and 10 at the start, the initial angular velocity is higher. For the Weissenberg number is equal to 10 this angular velocity will decrease, and for the Weissenberg number of 1 this does not happen. Figure 30b shows the angle θ as a function of strain for the extensional simulation with a fiber aspect ratio equal to 8 and with the initial orientation of 45 degrees. In these simulations, the influence of the Weissenberg number is not apparent.

6.3 Influence of β

This next section will investigate the influence of β. As explained in Chapter 4, a Newtonian solvent is added to stabilize the simulations. The parameter β is the ratio between the solvent viscosity and the total sum of

the viscosity as defined in Equation 11. This implies that for low values of β, the solvent viscosity is merely a fraction of the viscosity of the viscoelastic fluid itself. To isolate the influence of the effect of changing the β parameter, the other parameters α and Wi are kept constant. The values of β that have been studied are 0.001, 0.01, and 0.09. In shear flow the influence of this ratio β will be shown by means of three figures, one figure will show the orientation and two other figures will show the orientation angles as a function of strain. The influence of β in shear flow with a fiber aspect ratio of 2 can be seen in Figure 31, Figure 32 and Figure 33.

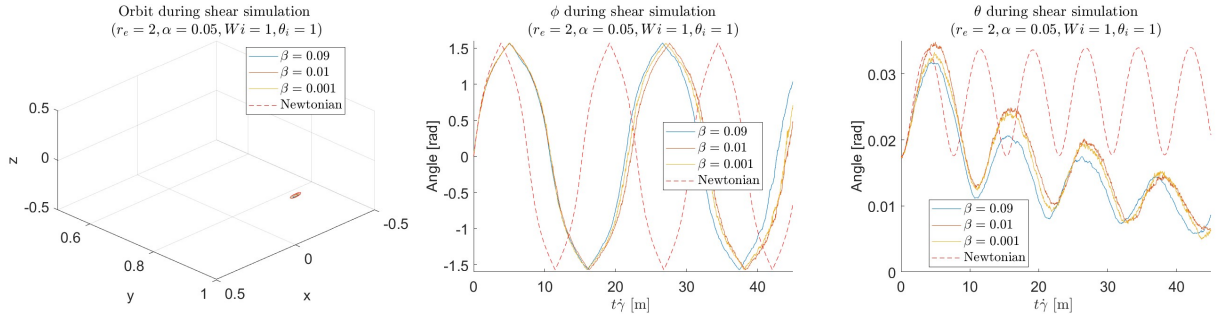

(a) Orientation of the fiber (b) The angle ϕ as a function of strain (c) The angle θ as a function of strain

Figure 31: Influence of the β for an initial orientation of $\theta = 1$ and an aspect ratio of 2

Figure 31 shows the influence of β in shear flow with initial angle θ equal to 1 for a fiber aspect ratio of 2. In these simulations, there is no dependence of β.

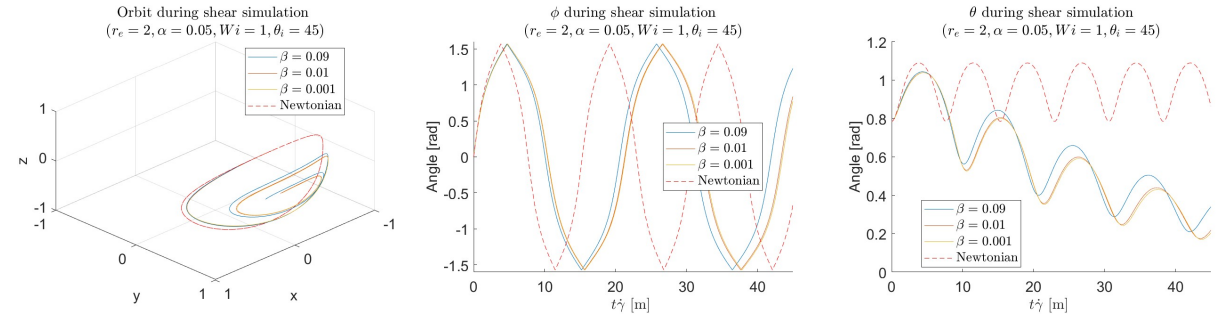

(a) Orientation of the fiber (b) The angle ϕ as a function of strain (c) The angle θ as a function of strain

Figure 32: Influence of the β for an initial orientation of $\theta = 45$ and an aspect ratio of 2

Figure 32 shows the influence of β in shear flow with initial angle θ equal to 45 degrees and a fiber aspect ratio equal to 2. The higher the value of β, the slower the spiraling toward the x-direction goes. Taking a β value of 0.01 and 0.001 results in the same simulation results for the orientation of the fiber.

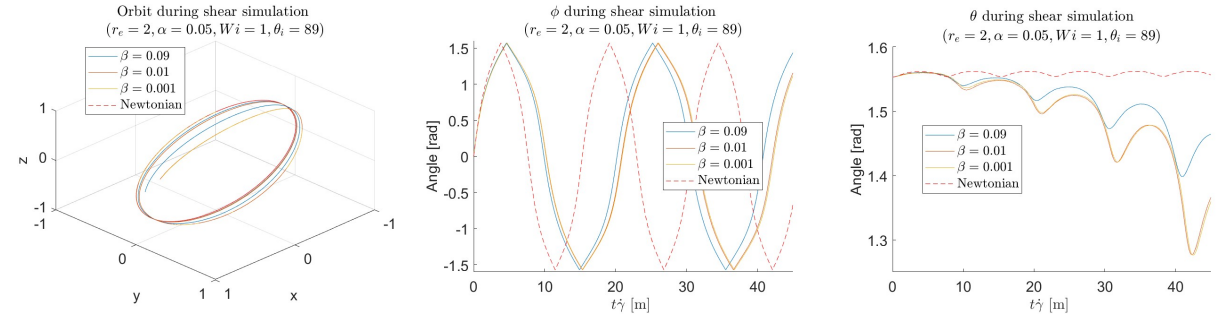

(a) Orientation of the fiber (b) The angle ϕ as a function of strain (c) The angle θ as a function of strain

Figure 33: Influence of the β for an initial orientation of $\theta = 89$ and an aspect ratio of 2

Figure 33 shows the influence of β for an initial angle θ of 89 degrees with a fiber aspect ratio of 2. Taking a β value of 0.01 and 0.001 results in the same simulation results. This implies that when the value of β is below 0.01 no influence of β is in the simulation compared to the other viscoelastic behavior.

A realistic hard fiber has a higher aspect ratio than 2. For this reason, the same set of simulations has been performed using a higher fiber aspect ratio of 8. The influence of β with an aspect ratio of 8 for the fiber is shown in Figure 34, Figure 35 and Figure 36.

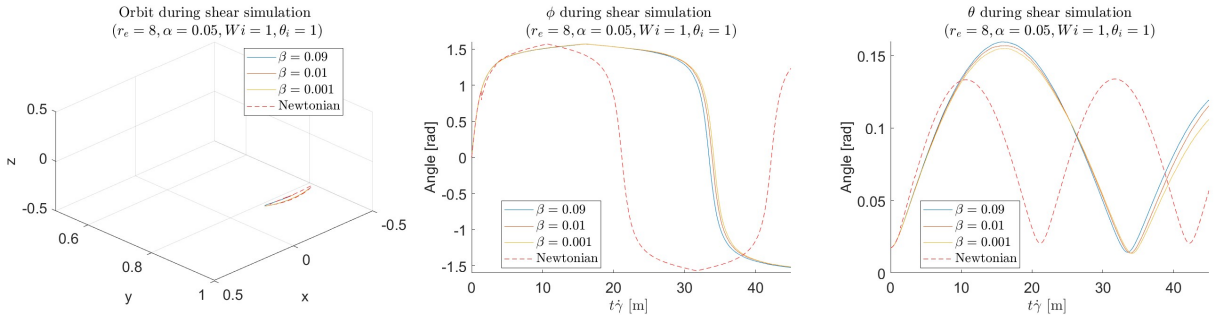

(a) Orientation of the fiber (b) The angle ϕ as a function of strain (c) The angle θ as a function of strain

Figure 34: Influence of the β for an initial orientation of θ = 1 and an aspect ratio of 8

Figure 34 shows the simulation results for the different values of β. This figure shows that there is no dependence of β.

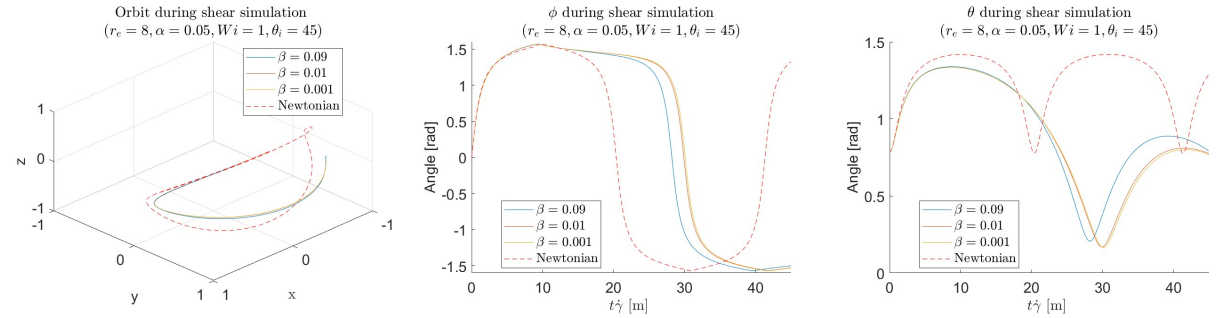

(a) Orientation of the fiber (b) The angle ϕ as a function of strain (c) The angle θ as a function of strain

Figure 35: Influence of the β for an initial orientation of θ = 45 and an aspect ratio of 8

Figure 35 shows the influence of β during shear simulation with a fiber aspect ratio of 8 and the initial angle θ equal to 45 degrees. Taking a β value of 0.01 and 0.001 results in the same simulation results. Taking a higher value of β results in a faster angular velocity. This implies that when the value of β is below 0.01 no influence of β is in the simulation compared to the other viscoelastic behavior.

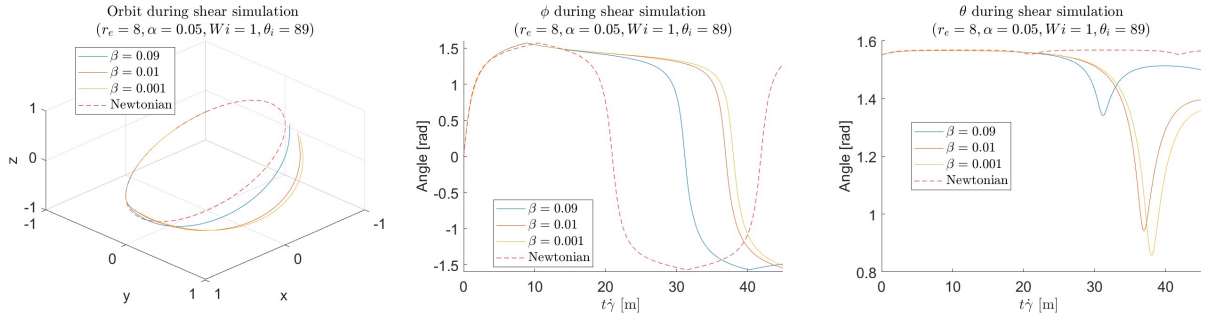

(a) Orientation of the fiber (b) The angle ϕ as a function of strain (c) The angle θ as a function of strain

Figure 36: Influence of the β for an initial orientation of θ = 89 and an aspect ratio of 8

Figure 36 shows the influence of β during shear simulation with a fiber aspect ratio of 8 and the initial angle θ equal to 89 degrees. The higher the value of β is, the higher the angular velocity is. Taking a β value of 0.01 and 0.001 results in the same simulation results. This implies that when the value of β is below 0.01 no influence of β is in the simulation compared to the other viscoelastic behavior.

Uniaxial extensional flow

Now, simulations are performed to investigate the influence of the ratio β on the fiber kinetics for uniaxial extensional flow. In uniaxial extension, the angle ϕ remains constant and is thus therefore not considered in the analysis. Likewise, the three-dimensional orientation in extensional flow will, for the used initial angles of θ, always show the fiber aligning with the flow direction. For this reason, this figure is not considered in the results. The initial angles of θ which are relevant for uniaxial extension are a starting angle of 1 degree and 45 degrees. The initial angle for ϕ still remains zero degrees. The influence of β in extensional flow for a fiber with an aspect ratio of 2 can be seen in Figure 37 and in Figure 38 with a fiber aspect ratio of 8.

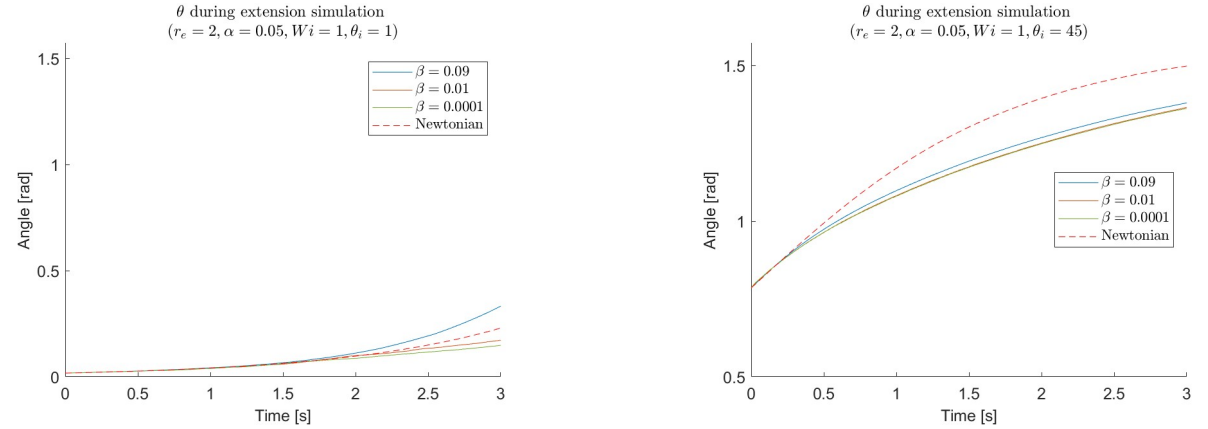

(a) The angle θ with initial angle θ equal to 1 degree (b) The angle θ with initial angle θ of 45 degrees

Figure 37: Influence of the β ratio in extensional flow for a fiber with aspect ratio 2

Figure 37a shows the simulation results for extensional flow with initial orientation angle of θ equal to 1 degree. The higher the value of β, the higher the angular velocity is. Figure 37b shows the simulation results with an initial orientation of 45 degrees for the angle θ. In these simulations, no dependence of β is apparent.

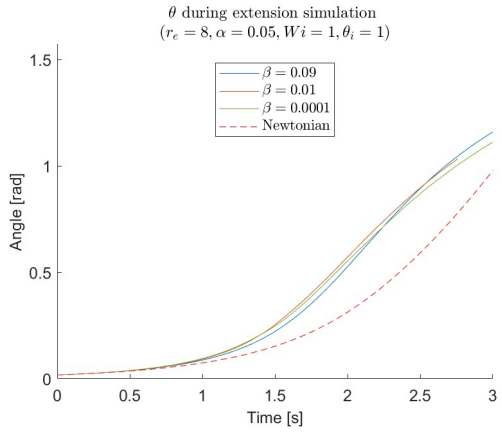

(a) The angle θ with initial angle θ equal to 1 degree

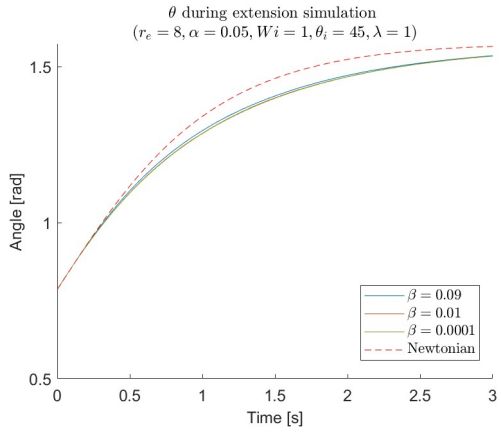

(b) The angle θ with initial angle θ of 45 degrees

Figure 38: Influence of the β ratio in extensional flow for a fiber with aspect ratio 8

Figure 38a shows the simulation results for the different values of β with initial orientation of 1 degree for the angle θ. Figure 38b shows the simulation results for the different values of β with initial orientation of 45 degrees for the angle θ. For both of these simulations, no dependence of β is apparent.

7 Conclusion

In this report, an investigation into the fiber orientation during the processing of fiber-filled polymer melts has been performed. First, single ellipsoidal fiber simulations subjected to shear flow in a Newtonian fluid are performed. These simulations are carried out using an in-house developed FEM package and are compared to the Jefferys orbit, this is the analytical solution for a single ellipsoidal fiber subject in simple shear flow, to obtain the error made in the simulations. Time convergence and mesh convergence studies are performed using the Jefferys orbits. After that, single spherocylindrical fiber simulations subjected to shear and uniaxial extensional flow have been performed to determine the influence of the characteristic fluid parameters on the orientation and rate of the orientation of the single fiber. These characteristic values are the viscosity ratio β, the non-linear parameter α, and the Weissenberg number.

The influence of the ratio β for the considered ratios is negligible compared to the other viscoelastic effects in the simulation. This shows that the Newtonian solvent does not influence the obtained simulation results, and thus the orientation kinetics observed are valid.

The α parameter has the most influence on the fiber orientation kinetics for fiber with larger aspect ratios in shear flow. The effect α shows itself in the regime where the fiber aligns with the shear flow direction. For higher value of α, the fiber will remain for less strain and thus less time at this aligned position. In Chapter 2.2 the effect of α was explained as how fast shear thinning takes place. For higher values of α more shear thinning will take place, the more shear thinning takes place the lower the viscosity is and thus the rotation of the fiber becomes easier. Allowing the fiber to move away from the shear flow direction faster.

The effect of the Weissenberg number is independent of the fiber aspect ratio for shear flow. For a high Weissenberg number of 10, the fiber will very slowly orient towards the shear flow axis. For a low Weissenberg number, the fiber will spiral toward the shear flow axis. These effects have also been observed by Geatanno and Hulsen [16]. The spiraling effect for the low Weissenberg number they mention as "log-rolling", was found for high Deborah numbers, and the slow movement towards the shear flow axis they found for low Deborah numbers. In extensional flow, the higher the Weissenberg number is, the faster the angular velocity is at the lower strain. At higher strains, this angular velocity decreases.

Recommendations

This section will discuss improvements that can be made to the simulations to be able to predict the fiber orientation more precisely during the processing of fiber-filled polymers. Both the extensional simulations and the shear flow simulations can be further improved. Above that, several other scenarios should be studied to be able to predict the fiber orientation during processing.

The effects in the extensional flow should be further investigated for higher strain values. The periodic box in extensional flow increased in the y-direction and decreased in x- and z-direction. This is for higher fiber aspect ratios a problem, since the box would decrease its dimensions further than the orientation of the fiber would allow for. This not only caused these numerical errors but also gives rise to the effects of neighboring fibers due to the assumed tri-periodic box. The rotation of the fiber at high strains could have been influenced by the neighboring fibers.

In shear flow, there were two cases observed where longer simulations would have been beneficial. For fibers with larger aspect ratios, the simulation should run for higher strain values to be able to capture more of the movement of these long fibers. Similarly, for higher Weissenberg numbers the angular velocity of the fiber is very low and should therefore the simulations should run for higher strain values. In the manufacturing of fiber-filled polymers, these high levels of strain could be reached depending on the product and production method.

Another improvement that can be made is simulating the orientation kinetics of the fiber for different viscoelastic models. This report has focused on the effect of a Giesekus viscoelastic fluid, but several other viscoelastic fluid models exist that describe the behavior of polymer melts. These different viscoelastic fluid models each have a difference in the constitutive equation for the extra stress tensor, which could result in different orientation kinetics and different important parameters.

When making fiber-filled polymer products, the interaction between multiple fibers could play a role in

the orientation kinematics. A fiber-filled polymer contains many fibers, which are generally not uniformly aligned. This is not considered in this report. The interaction of the fibers might also depend on the characteristic viscoelastic properties, and that should be investigated to be able to precisely predict the orientation of fibers in a production process.

The simulations have thus far not considered the influence of temperature. In the processing of polymers, the polymers are heated up to have the polymers in fluid form. In the processing, the polymers will cool down, resulting in the final end product. During this cooling down process, the orientation of the fibers might be influenced further due to the anisotropic material behavior of polymers. This could result in the end product having a different orientation once the polymer melt has been cooled down.

In polymer processing techniques, the polymer flow is obstructed in many ways. These obstructions guide the flow and make sure that the polymer obtains the form of the desired end product. Obstructions will have an influence on the flow of the fluid, and it is therefore likely to have an influence on the fiber orientation kinetics.

With each of these above-motioned recommendations, the local fiber orientation of a fiber-filled polymer product can be more accurately simulated. And will thus result in better predictability of the mechanical properties of fiber-filled polymer products.

A Derivation of $\dot{\vec{q}}$

To obtain the derivative of the orientation vector, the vector can be differentiated. Since the evolution equation of θ and ϕ are known, Equation 14 and Equation 13 respectfully, the orientation vector can be differentiated by

$$\dot{\vec{q}} = \frac{d}{dt}\vec{q}. \tag{24}$$

This leads to

$$\dot{\vec{q}} = \begin{pmatrix} \dot{\theta}\cos(\theta)\sin(\phi) + \dot{\phi}\sin(\theta)\cos(\phi) \\ \dot{\theta}\cos(\theta)\cos(\phi) - \dot{\phi}\sin(\theta)\sin(\theta) \\ -\dot{\theta}\sin(\theta) \end{pmatrix} \tag{25}$$

for the expression of $\dot{\vec{q}}$.

B Matlab Code Analytical solution

```
%% Definition of input variables
gammadot = 1;                       % Shear rate
r = 2;                              % Aspect ratio
dt = 0.01;                          % Time step
tmax = 10;                          % End time
% Angle input
phi_0 =  0 * pi / 180;              % Starting angle
theta_0 = 45 * pi / 180;            % Starting angle

% Vector input (does not have to be normalized)
lambda_start = [1;0;1];             % Starting potition vector

Input_used = 'vector'; %'vector' or 'angle' to be used to select

%% Quick calculations
% For input being angles
lambda_0 = [sin(theta_0)*sin(phi_0);sin(theta_0)*cos(phi_0);cos(theta_0)];

% For input being direction vector
lambda_st = lambda_start/norm(lambda_start);        %Normalize the vector
theta_start = acos(lambda_st(3));                   %Finding the first angle
phi_start = asin(lambda_st(1)/sin(theta_start));    %Finding the second angle

%% Selection of input (Angles or directional vector)
% Picking the prefered input - based on vector
Input_used_vector = strcmp(Input_used,'vector');
Input_used_angle  = strcmp(Input_used,'angle');
if Input_used_vector == 1
lambda_init = lambda_st;
phi_init = phi_start;
theta_init = theta_start;
end
% Picking the prefered input - based on angles
if Input_used_angle == 1
lambda_init = lambda_0;
phi_init = phi_0;
theta_init = theta_0;
end

C = tan(theta_init)/(r*(r^2*cos(phi_init)^2+sin(phi_init)^2)^-0.5);

%% Analytical solution
steps = nsteps;
t = linspace(0,tmax,steps);

phi = atan(r*tan((gammadot*t)/(r+r^(-1))));

% Compensating for the inverse tangent not returning the full domain
for index = 2:1:steps
    if phi(index) < 0
        phi(index) = phi(index) + pi;
    end

    if phi(index-1) - phi(index) > 0.95*pi
        phi(index) = phi(index) + pi;
    end

    if phi(index) - phi(index-1) < -3
        phi(index) = phi(index) - pi;
    end

end

theta = atan((C * r) ./ ((r^2*cos(phi).^2+sin(phi).^2).^(1/2)));

lambda = [sin(theta).*sin(phi); sin(theta).*cos(phi); cos(theta)];
```

C Matlab Code Integration solution

```
%% Definition of input variables
gammadot = 1;                       % Shear rate
r = 2;                              % Aspect ratio
dt = 0.01;                          % Time step
tmax = 10;                          % End time

% Angle input
phi_0 =  0 * pi / 180;              % Starting angle
theta_0 = 45 * pi / 180;            % Starting angle

% Vector input (does not have to be normalized)
lambda_start = [1;0;1];             % Starting potition vector

Input_used = 'vector';              %'vector' or 'angle' to be used to select

%% Quick calculations
% For input being angles
lambda_0 = [sin(theta_0)*sin(phi_0);sin(theta_0)*cos(phi_0);cos(theta_0)];

% For input being direction vector
lambda_st = lambda_start/norm(lambda_start);        %Normalize the vector
theta_start = acos(lambda_st(3));                   %Finding the first angle
phi_start = asin(lambda_st(1)/sin(theta_start));    %Finding the second angle

%% Selection of input (Angles or directional vector)
% Picking the prefered input - based on vector
Input_used_vector = strcmp(Input_used,'vector');
Input_used_angle  = strcmp(Input_used,'angle');
if Input_used_vector == 1
lambda_init = lambda_st;
phi_init = phi_start;
theta_init = theta_start;
end
% Picking the prefered input - based on angles
if Input_used_angle == 1
lambda_init = lambda_0;
phi_init = phi_0;
theta_init = theta_0;
end

%% Intergral form
time = 0:dt:tmax;
nsteps = length(time);


% Building empty arrays
theta_d=zeros(nsteps,1);
phi_d=zeros(nsteps,1);
theta_dot=zeros(nsteps,1);
phi_dot=zeros(nsteps,1);
phi_d2=zeros(nsteps,1);

% Inserting intial value's if applicable
theta_d(1) = theta_init;
phi_d(1) = phi_init;
lambda_d(:,1)= lambda_init;

for i = 2:nsteps

    % update theta
    theta_dot(i) = (r^2-1)/(r^2+1)*gammadot/4*sin(2*theta_d(i-1))*sin(2*phi_d(i-1));

    % 2nd order Adam-Bashford for theta
    if i == 2
        theta_d(i) = theta_d(i-1) + dt*theta_dot(i);
    else
        theta_d(i) = theta_d(i-1) + dt*(3/2*theta_dot(i)-1/2*theta_dot(i-1));
    end

    % update phi
    phi_dot(i) = gammadot/2*(1+(r^2-1)/(r^2+1)*cos(2*phi_d(i-1)));

    % 2nd order Adam-Bashford for phi
    if i == 2
        phi_d(i) = phi_d(i-1) + dt*phi_dot(i)    ;
```

```
76          else
77              phi_d(i) = phi_d(i-1) + dt*(3/2*phi_dot(i)-1/2*phi_dot(i-1));
78          end
79
80          phi_d2(i) = wrapTo2Pi(phi_d(i));
81
82          % Computing lambda based on the new angles
83          lambda_d(:,i) = [sin(theta_d(i))*sin(phi_d(i)); sin(theta_d(i))*cos(phi_d(i)); ...
                cos(theta_d(i))];
84      end
```

References

[1] Callister W.D. and Rethwisch D.G., *Materials science and engineering: an introduction*. John Wiley & Sons, 10th ed., 2018.

[2] L. A. Goettler and K. S. Shen, "Short Fiber Reinforced Elastomers," *Rubber Chemistry and Technology*, vol. 56, pp. 619–638, 7 1983.

[3] J. F. Agassant, F. Pigeonneau, L. Sardo, and M. Vincent, "Flow analysis of the polymer spreading during extrusion additive manufacturing," *Additive Manufacturing*, vol. 29, p. 100794, 10 2019.

[4] S. L. Belcher, "Blow Molding," *Applied Plastics Engineering Handbook: Processing, Materials, and Applications: Second Edition*, pp. 265–289, 1 2017.

[5] S. Onaka, "Hencky strain as a measure to evaluate large deformations caused by giant straining processes," *Nippon Kinzoku Gakkaishi/Journal of the Japan Institute of Metals*, vol. 74, pp. 165–170, 3 2010.

[6] D. J. Acheson, *Elementary fluid dynamics*. Clarendon Press, 1990.

[7] A. E. Likhtman, "Viscoelasticity and Molecular Rheology," *Polymer Science: A Comprehensive Reference, 10 Volume Set*, vol. 1, pp. 133–179, 1 2012.

[8] H. Giesekus, "A SIMPLE CONSTITUTIVE EQUATION FOR POLYMER FLUIDS BASED ON THE CONCEPT OF DEFORMATION-DEPENDENT TENSORIAL MOBILITY," *Journal 01 Non-Newronran Flurd Mechanrcs, I I*, p. 69, 1982.

[9] Jeffery G. B., "The motion of ellipsoidal particles immersed in a viscous fluid," *Proceedings of the Royal Society of London. Series A, Containing Papers of a Mathematical and Physical Character*, vol. 102, pp. 161–179, 11 1922.

[10] S. Kim and S. J. Karrila, "Resistance and Mobility Relations," in *Microhydrodynamics*, ch. 5, pp. 107–145, Elsevier, 1991.

[11] R. Guénette and M. Fortin, "A new mixed finite element method for computing viscoelastic flows," *Journal of Non-Newtonian Fluid Mechanics*, vol. 60, pp. 27–52, 10 1995.

[12] A. C. Bogaerds, A. M. Grillet, G. W. Peters, and F. P. Baaijens, "Stability analysis of polymer shear flows using the eXtended Pom–Pom constitutive equations," *Journal of Non-Newtonian Fluid Mechanics*, vol. 108, pp. 187–208, 12 2002.

[13] A. N. Brooks and T. J. Hughes, "Streamline upwind/Petrov-Galerkin formulations for convection dominated flows with particular emphasis on the incompressible Navier-Stokes equations," *Computer Methods in Applied Mechanics and Engineering*, vol. 32, pp. 199–259, 9 1982.

[14] R. Fattal and R. Kupferman, "Constitutive laws for the matrix-logarithm of the conformation tensor," *Journal of Non-Newtonian Fluid Mechanics*, vol. 123, pp. 281–285, 11 2004.

[15] M. A. Hulsen, R. Fattal, and R. Kupferman, "Flow of viscoelastic fluids past a cylinder at high Weissenberg number: Stabilized simulations using matrix logarithms," *Journal of Non-Newtonian Fluid Mechanics*, vol. 127, pp. 27–39, 4 2005.

[16] G. D'Avino, M. A. Hulsen, F. Snijkers, J. Vermant, F. Greco, and P. L. Maffettone, "Rotation of a sphere in a viscoelastic liquid subjected to shear flow. Part I: Simulation results," *Journal of Rheology*, vol. 52, pp. 1331–1346, 11 2008.